https://doi.org/10.5194/egusphere-2025-2606
Preprint. Discussion started: 28 July 2025

From grid to ground: How well do gridded products represent soil moisture dynamics in natural ecosystems during precipitation events?

Daniel A. Núñez-Ibarra[1, 2, 5], Mauricio Zambrano-Bigiarini[3, 1], and Mauricio Galleguillos[4, 5, 1]

[1]Center for Climate and Resilience Research, Universidad de Chile, Santiago, Chile.
[2]Master's Degree in Territorial Management of Natural Resources (GESTREN) Universidad de Chile, Santiago, Chile.
[3]Department of Civil Engineering, Universidad de la Frontera, Temuco, Chile.
[4]Faculty of Engineering and Sciences, Universidad Adolfo Ibáñez, Santiago, Chile.
[5]Data Observatory Foundation, ANID Technology Center, Santiago, Chile

Correspondence: Mauricio Zambrano-Bigiarini (mauricio.zambrano@ufrontera.cl) and Mauricio Galleguillos (m.galleguillos@uai.cl)

Abstract. Soil moisture (SM) is a critical variable governing land–atmosphere interactions and influencing ecohydrological and climatic processes. Despite substantial progress in estimating SM through remote sensing and land surface models, considerable uncertainties still remain, especially in near-natural and poorly monitored ecosystems interacting with deeper soil layers. In this study, the performance of four state-of-the-art gridded SM products (SPL4SMAU, GLDAS-Noah, ERA5 and ERA5-Land) is evaluated against in situ observations at ten natural monitoring sites in central and southern Chile, covering different hydroclimatic conditions (five semi-arid and five humid sites). The evaluation is performed at a 3-hourly temporal resolution, using well-known statistical metrics of performance, including unbiased root mean square error (ubRMSE), modified Kling–Gupta efficiency (KGE′), deseasonalised Spearman's rank correlation coefficient (ρ), and percent bias (PBIAS), each applied separately for surface soil moisture (SSM) and root zone soil moisture (RZSM). Finally, the dynamic SM responses to precipitation events is evaluated using rising time (RT) and amplitude (A) SM signatures during the first and the most intense precipitation events of the year.

Our results show that ERA5 and ERA5-Land consistently outperform SPL4SMAU and GLDAS-Noah on most metrics and in most regions, with ERA5-Land being particularly strong in humid areas. However, SPL4SMAU achieved the best SSM performance in selected northern arid locations, based on KGE′; while GLDAS-Noah performed the worst overall, with the exception of moderate correlation values in southern RZSM. During the first precipitation event of the year, all products systematically overestimated both rising times and amplitudes in the arid north, indicating challenges in capturing SM responses under dry antecedent conditions. In contrast, all the gridded products aligned more closely with in situ measurements during intense precipitation events, particularly in humid regions. Our findings suggest that both ERA5 and ERA5-Land are valuable datasets for monitoring SM variability in near-natural and data-scarce ecosystems, while highlighting the value of event-based SM signatures to complement traditional performance metrics. Finally, we recommend the use of the deseasonalised Spearman rank correlation to better detect inconsistencies in temporal dynamics, especially in regions with strong seasonal cycles, such as arid environments.

https://doi.org/10.5194/egusphere-2025-2606
Preprint. Discussion started: 28 July 2025

1 Introduction

A sound representation of the spatio-temporal dynamics of soil moisture (SM) is essential for improving our understanding of eco-hydrological processes and for enhancing the accuracy of hydrological and climate models, particularly in regions with complex hydroclimatic conditions. SM has a direct influence on important hydrological processes such as infiltration, runoff, and evaporation; mediates the exchange of energy and mass between land and atmosphere (Vereecken et al., 2022), and actively regulates the water resources available to vegetation in space and time (Peng et al., 2021). Surface soil moisture (SSM) refers to the moisture content within the top layer of soil, typically the first 5–10 cm. In contrast, root zone soil moisture (RZSM) refers to the moisture available in deeper soil layers (typically 100 cm or more), where plant roots can extract water. Understanding the dynamic fluctuations of these two variables across different ecosystems is essential for improving drought monitoring, hydrological modelling, long-term water availability estimates, and water resources management, among others.

Dynamic fluctuations of SSM and RZSM are primarily governed by changes in precipitation (P), the primary source of soil water recharge. In particular, the spatial and temporal variability of SSM is directly influenced by the frequency and intensity of P events, affecting its immediate availability in the top soil layer (Zheng et al., 2022b; Xi et al., 2023). In contrast, RZSM responds to precipitation changes with a delay, as water must infiltrate into deeper soil layers before being stored in the root zone (Tian et al., 2019). This temporal difference plays a fundamental role in water tranfers in the soil, particularly in regions with irregular precipitation patterns, where RZSM retains water for extended periods of time (Hao et al., 2019; Räsänen et al., 2020).

Accurately representing SM dynamics across different ecosystems requires reliable and spatially continuous data. SM data are derived from diverse sources, including in situ measurements, satellite observations, land surface models (LSMs), and re-analysis datasets. In situ measurements provide highly accurate data, although their spatial coverage is limited, with monitoring networks concentrated predominantly in the Northern Hemisphere (Beck et al., 2021). Notable networks such as TERRENO (Zacharias et al., 2011), Oznet (Smith et al., 2012), COSMOS-UK (Evans et al., 2016), and the International Soil Moisture Network (ISMN; Dorigo et al., 2021) provide valuable long-term datasets. However, most of these networks only provide estimates for the first few centimetres of the soil profile (Dorigo et al., 2021), have limited coverage in the Southern Hemisphere, and rarely include natural ecosystems with minimally disturbed soils.

On the other hand, satellite observations provide a consistent and (near-)global estimates of SSM at varying spatial and temporal resolutions. Passive microwave sensors, such as those onboard Soil Moisture Active Passive (SMAP; Entekhabi et al., 2010b) and the Advanced Microwave Scanning Radiometer 2 (AMSR2; Imaoka et al., 2012; Parinussa et al., 2015), estimate SM by detecting variations in land surface emissivity; while active microwave sensors, like those used in Sentinel-1, leverage radar backscatter to retrieve SSM at higher spatial resolution (Paloscia et al., 2013). However, satellite-based SM retrievals are generally limited to the top soil layer, typically within the upper 10 cm, and are affected by factors such as vegetation cover and radio frequency interference. As a result, integrating multiple data sources is often necessary to enhance their accuracy (Peng et al., 2021; Dorigo et al., 2021). More critically, satellite observations cannot capture SM dynamics in deeper soil layers (i.e., in the RZSM), which is vital for understanding long-term water availability and plant growth dynamics.

https://doi.org/10.5194/egusphere-2025-2606
Preprint. Discussion started: 28 July 2025

To address some of the limitations of satellite estimates, in the last decades several LSMs and reanalysis datasets have been used to estimate SM across multiple soil depths. Land surface models, such as NOAH-MP (Niu et al., 2011) and the Community Land Model (CLM; Lawrence et al., 2019), simulate physical, chemical, and biological processes at the land–atmosphere interface by solving equations that govern the balances of energy, water, momentum, and carbon. Their inputs typically include atmospheric forcing data (e.g., P, radiation, wind, temperature) and they simulate SM at multiple depths based on soil, vegetation, and terrain characteristics (Van Den Broeke et al., 2018; Zhuo et al., 2019). On the other hand, reanalysis like ERA5-Land (Muñoz-Sabater et al., 2021) and MERRA-2 (Gelaro et al., 2017) aim to create a comprehensive and time-consistent representation of atmospheric, oceanic, and land variables, by using data assimilation to combine observations (e.g., satellites, weather stations) with output from a global numerical weather prediction (NWP) model. Land surface models are often embedded within a reanalysis system to simulate land variables, resulting in high temporal and spatial resolution datasets covering last decades (Gelaro et al., 2017; Hersbach et al., 2020). However, the accuracy of reanalysis depends on the quality of the assimilated observations and model parameterisations, requiring validation against in situ measurements to improve regional applicability (Beck et al., 2021).

Despite advances in LSMs, satellite observations, and reanalysis datasets, the limited availability of in situ SM data in the Southern Hemisphere poses a significant challenge for validating these (near-global) estimates. The lack of a comprehensive ground-based SM network hinders our ability to analyse SM variability, particularly in heterogeneous landscapes. Furthermore, while gridded SM products have demonstrated good performance in studies with many observations (Beck et al., 2021; Lai et al., 2023; Zheng et al., 2023, 2024; Brocca et al., 2024), their applicability in data-sparse regions remains uncertain and requires evaluation before widespread adoption.

Direct evaluation of gridded SM datasets against in situ observations are complicated by differences in spatial and temporal resolution, which might lead to misinterpretations of SM dynamics (Colliander et al., 2018). In addition, time series comparisons for medium to long-term periods fail to capture the complete SM dynamics, as they do not adequately reflect short-term fluctuations and retention patterns that influence hydrological and ecological processes (Araki et al., 2022). To overcome these limitations, SM signatures have emerged over the last decade as valuable metrics for analysing gridded datasets and assessing the dynamic response of SM to precipitation events in different ecological contexts (Branger and McMillan, 2020; Araki et al., 2022). In contrast to traditional full-time series comparisons, SM signatures allow a more detailed characterisation of SM dynamics and provide insights into key hydrological soil processes, such as wetting and drying cycles, water retention and infiltration (Branger and McMillan, 2020; Araki et al., 2022, 2023). With climate projections suggesting further declines in SM and increasing aridification in semi-arid regions (such as central Chile) by the end of the 21st century (Lai et al., 2023), an exhaustive evaluation of the SM responses to P events is critical to better understand the spatio-temporal dynamics of SM.

Chile's diverse ecosystems, ranging from semi-arid shrublands to temperate native forests, exhibit distinct water retention and infiltration processes (Bown et al., 2018); making the region an excellent natural laboratory for evaluating soil moisture dynamics under contrasting hydroclimatic conditions. For instance, the limited water retention capacity of soils in the semi-arid Petorca River Basin leads to rapid SM depletion after the occurrence of P events (Muñoz et al., 2020). In contrast, the deep soils and dense native vegetation typical of the Trancura River Basin allow for longer water storage (Frêne et al., 2020).

https://doi.org/10.5194/egusphere-2025-2606
Preprint. Discussion started: 28 July 2025

By evaluating gridded SM products under such contrasting hydroclimatic and ecological conditions, this study will contribute to filling the existing gap in their assessment on natural, undisturbed ecosystems, especially in under-represented regions of the Southern Hemisphere. Our results will help to improve our understanding of eco-hydrological processes and increase the accuracy of hydrological and climatic modelling applications. To this end, we present the first evaluation of 3-hourly gridded SM datasets for native ecosystems in South America, focusing on their ability to capture surface and root zone dynamics during precipitation events. Specifically, we address the following two research questions:

- How well do 3-hourly gridded products represent SSM and RZSM dynamics in natural ecosystems of the Southern Hemisphere during precipitation events?
- How reliably do gridded datasets represent SM signatures across diverse hydroclimatic conditions?

2 Datasets

2.1 Study area

The study area is situated in central-southern Chile, between 32.01°S and 39.64°S, and is characterised by a wide variety of elevations, land cover, soil properties, and aridity, as shown in Figure 1. In the north, the Petorca River Basin (PRB, in the Valparaíso region) is semi-arid, dominated by sparse shrublands and low P amounts. The Mapocho en Los Almendros River Basin (MRB, in the Metropolitan region) transitions to a moderate climate with shrublands and agricultural fields. The Cauquenes River Basin (CRB, in the Maule and Ñuble regions) is more humid, with a predominance of pine plantations and native shrublands. Further south, the Trancura River Basin (TRB, in the Araucanía region) is characterized by dense native forests, high P amounts, and elevations exceeding 2,000 m a.s.l. The aridity index ($AI = P/PET$, where PET stands for potential evapotranspiration), derived from the Global-AI-PET-v3 dataset (Zomer et al., 2022), emphasises the pronounced climatic gradient in the study area, which ranges from arid conditions in the PRB (AI < 0.3) to very humid conditions in the TRB (AI > 1.25).

2.2 Gridded SM datasets

In this study we evaluated four state-of-the-art SM gridded datasets: i) ERA5 (Hersbach et al., 2020), ii) ERA5-Land (Muñoz-Sabater et al., 2021), iii) GLDAS-Noah (Xing et al., 2021), and iv) SMAP-SPL4SMAU (Reichle et al., 2017a, b), which are briefly described in the following lines.

2.2.1 ERA5

ERA5 is the fifth-generation reanalysis product developed by the European Centre for Medium-Range Weather Forecasts (ECMWF; Hersbach et al., 2020). It uses the Hydrology Tiled ECMWF Scheme for Surface Exchanges over Land (HTESSEL) to effectively simulate SM dynamics, capturing complex interactions among precipitation, evaporation, infiltration, and runoff.

https://doi.org/10.5194/egusphere-2025-2606
Preprint. Discussion started: 28 July 2025

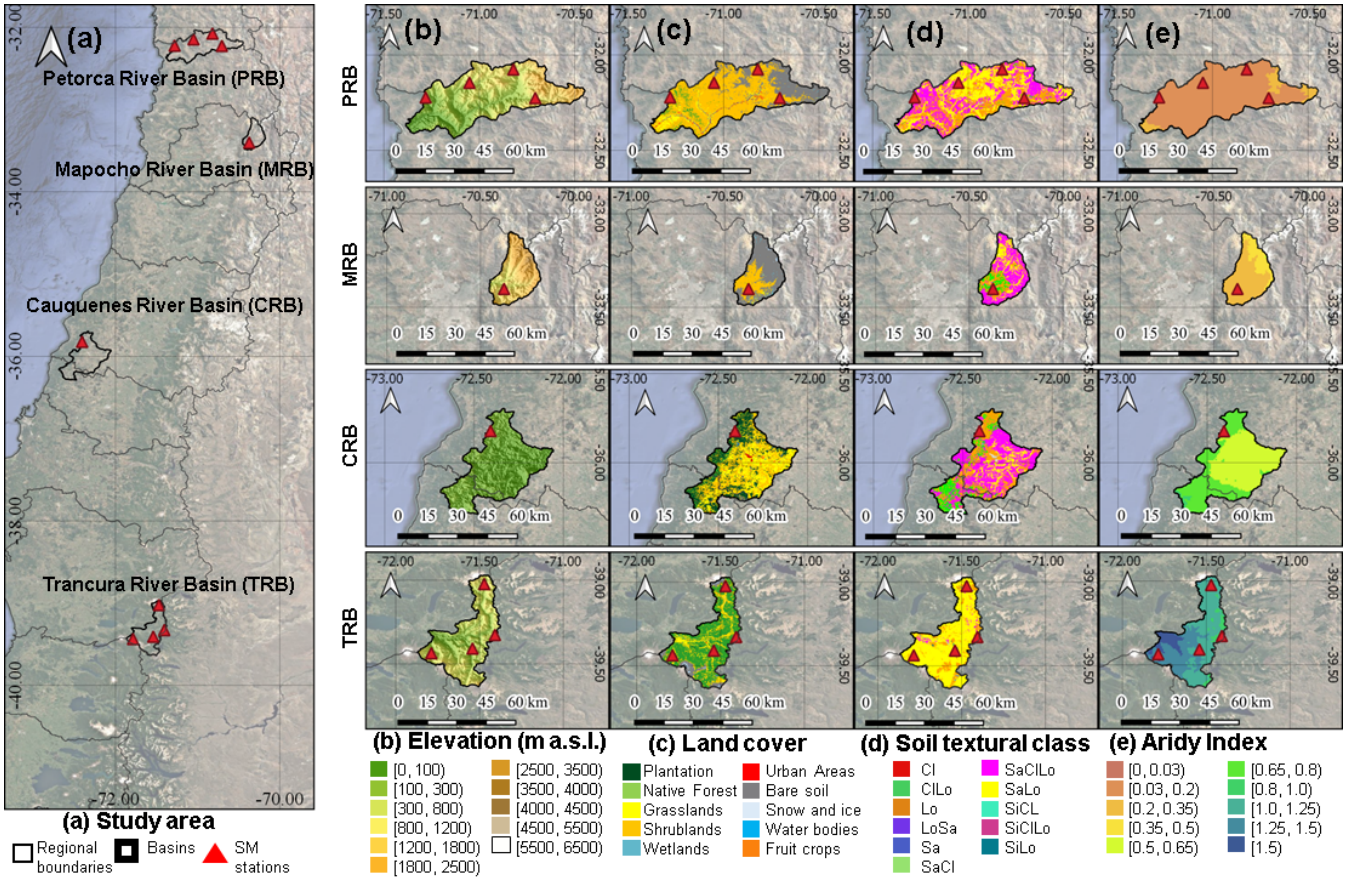

Figure 1. Study area: (a) catchment location (CAMELS-CL; Alvarez-Garreton et al., 2018); (b) elevation (SRTMv4.1; Jarvis et al., 2008); (c) land cover classification (LC.V2; Galleguillos et al., 2024); (d) soil properties (CLSoilMaps; Dinamarca et al., 2023); and (e) aridity index ($AI = P/PET$) 1970-2000 (Global-AI-PET-v3; Zomer et al., 2022). Basemap imagery © Google Earth (Google LLC, 2024).

These hydrological processes are modelled through advanced equations that elucidate the energy and water exchanges between soil, vegetation, and the atmosphere. A key feature of ERA5 is the integration of remote sensing data for SM over land, using backscatter data from C-band scatterometers. Although SM retrievals from satellite sources such as the Advanced Scatterometer (ASCAT; Wagner et al., 2013) are not directly assimilated into ERA5, they have a significant impact on the modelled surface fluxes and soil states, enhancing the accuracy of the simulated SM. This dataset contains high-resolution data on volumetric soil water content in four vertical layers: 0–7 cm for SSM and 7-28 cm, 28-100 cm and 100-289 cm for RZSM; with an hourly temporal resolution and a native spatial resolution of 31 km, from 1940 to present. This high-resolution and globally uniform coverage proves essential for various applications, ranging from hydrological modelling to agricultural planning. Here we used the ERA5 single-levels reanalysis data, from the Copernicus Climate Data Store (Hersbach et al., 2023).

https://doi.org/10.5194/egusphere-2025-2606
Preprint. Discussion started: 28 July 2025

2.2.2 ERA5-Land

ERA5-Land is a reanalysis dataset that further refines the land component of ERA5, providing a high-resolution and consistent overview of land variables over several decades (Muñoz-Sabater et al., 2021). ERA5-Land operates at a spatial resolution of 0.10° and extends from 1950 to present, using the HTESSEL as land surface model, driven by downscaled ERA5 meteorological data to account for elevation differences (Muñoz-Sabater, 2019). In contrast to ERA5, which involves indirect assimilation of observational data, ERA5-Land relies exclusively on physical modelling within HTESSEL to simulate SM dynamics in the four vertical soil layers without direct data assimilation. This method ensures a complete derivation of SM from high-resolution meteorological data, which maintains the physical consistency of the land surface simulations and avoids artifacts due to corrections of the observational data. This dataset provides volumetric soil water content in the same four vertical layers of ERA5, allowing a more detailed visualisation of the local-scale variations of SM, as influenced by topography, vegetation and soil properties (Muñoz-Sabater et al., 2021; Nogueira et al., 2020; Liu et al., 2024). Here we used the hourly data obtained from the Copernicus Climate Data Store (Muñoz-Sabater et al., 2021).

2.2.3 SMAP SPL4SMAU

The Soil Moisture Active Passive (SMAP; Entekhabi et al., 2010a) Level-4 Soil Moisture (Reichle et al., 2014) product provides comprehensive global estimates of SM at the surface (0–5 cm) and in the root zone (0–100 cm) with a spatial resolution of 9 km, updated every 3 hours from March 2015 onwards. This dataset integrates L-band brightness temperature observations from the SMAP radiometer into the Catchment Land Surface Model (CLSM; Reichle et al., 2022b). The data assimilation system used in this product corresponds to the Goddard Earth Observing System Version 7 (GEOS-5 LDAS), which contains a spatially distributed ensemble Kalman filter with a 3-hourly update interval for the integration of observations and model simulations (Rienecker et al., 2008; Reichle et al., 2022b). The meteorological surface data of the GEOS-5 Forward Processing (FP) system drives the CLSM model, using the daily CPCU precipitation observations to adjust and scale the GEOS-5 FP precipitation data to the climatology of the Global Precipitation Climatology Project version 2.2 (GPCP v2.2; Adler et al., 2020). The SMAP L4 product also integrates soil properties from the Harmonized World Soil Database (HWSD) V1.2 (Wieder et al., 2014) and land cover data from the GlobCover 2009 (Arino et al., 2012). Here we used the SMAP L4 Global 3-hourly 9 km EASE-Grid grid Surface and Root Zone Soil Moisture Analysis Update (SPL4SMAU; Reichle et al., 2022a) data version 7 available from the NSIDC (https://nsidc.org/data/spl4smau/versions/7).

2.2.4 GLDAS-Noah

The Global Land Data Assimilation System (GLDAS; Rodell et al., 2004) NOAH version 2.1 (Beaudoing et al., 2020) is developed by NASA's Goddard Earth Sciences Data and Information Services Center (GES DISC), and delivers optimal land surface states and fluxes without incorporating data assimilation. Operating offline, the Noah Land Surface Model is driven by a combination of atmospheric fields from NOAA's Global Data Assimilation System, precipitation data from the Global Precipitation Climatology Project (GPCP) V1.3 Daily Analysis (Huffman et al., 1997), and radiation inputs from AGRMET

https://doi.org/10.5194/egusphere-2025-2606
Preprint. Discussion started: 28 July 2025

(Meng et al., 2001). Soil moisture dynamics are represented in a four-layer soil column, simulated by the diffusive form of the Richards equation. Additionally, GLDAS-Noah utilizes a hybrid STATSGO/FAO World Soil Map (Dy and Fung, 2016) and applies a modified MODIS vegetation classification scheme with 20 categories (Rui et al., 2021). Unlike ERA5, the GLDAS-Noah product is available at 3-hour intervals. Here we used the GLDAS-Noah v2.1 data from GES DISC (NASA/GSFC/HSL, 2020).

Table 1. Gridded SM products used in this study.

Product	Data type	Land surface Model	Soil layers [cm]	Temporal Coverage	Spatial and temporal resolution	Landcover product	References
ERA5	Reanalysis	(H)TESSEL	0–7, 7–28, 28–100, 100–289	1940–present	0.25°, hourly	GLCC v1.2	Hersbach et al. (2020)
ERA5-Land	Reanalysis	(H)TESSEL	0–7, 7–28, 28–100, 100–289	1950–present	0.10°, hourly	GLCC v1.2	Muñoz-Sabater (2019); Muñoz-Sabater et al. (2021)
SMAP-SPL4SMAU	LSM*	GEOS	0–5, 0–100	2015–present	9 km, 3-hourly	GlobCover 2009	Reichle et al. (2017a, 2022a)
GLDAS-Noah V2.1	LSM	NOAH	0–10, 10–40, 40–100, 100–200	2000–present	0.25°, 3-hourly	MCD12Q1	Rodell et al. (2004); NASA/GSFC/HSL (2020)

2.3 In situ SM observations

To evaluate the four gridded SM datasets descried in Section 2.2, we used the Kimün-Ko SM monitoring network, which has been fully operational since 2022. It was developed to characterise SM variability in undisturbed ecosystems of central and southern Chile, which are under-represented in global monitoring networks that primarily focus on agricultural areas in the Northern Hemisphere. (Dorigo et al., 2021; Beck et al., 2021).

The Kimün-Ko network estimate SM dynamics using TEROS 10 and TEROS 12 capacitance sensors, installed at depths ranging from 10 to 200 cm and connected to ZL6 data loggers for high-frequency data acquisition. Ten monitoring sites were selected within the study area (Figure 2); five in the semi-arid north (PRB and MRB, Figure 2.b) and five in the humid south (CRB and TRB, Figure 2.c); to reflect a range of hydroclimatic conditions and land cover types. All ten SM monitoring sites are situated in areas classified as Sandy Loam (SaLo) based on CLSoilMaps (Dinamarca et al., 2023). The placement of each station also ensures spatial correspondence with the cells of the gridded SM products being evaluated. At each site, volumetric soil water content (m^3/m^3) is recorded at an hourly temporal resolution. Details of sensor depths and site characteristics are summarised in tables 2 and 3, respectively. Each monitoring site is equipped with a rain gauge that is close enough to the SM sensor to be considered representative of the precipitation falling over the site. Table 2 show a summary of the sensor depths, location, elevation and land cover of each monitoring site, while Table 3 summarise the soil texture in each site.

https://doi.org/10.5194/egusphere-2025-2606
Preprint. Discussion started: 28 July 2025

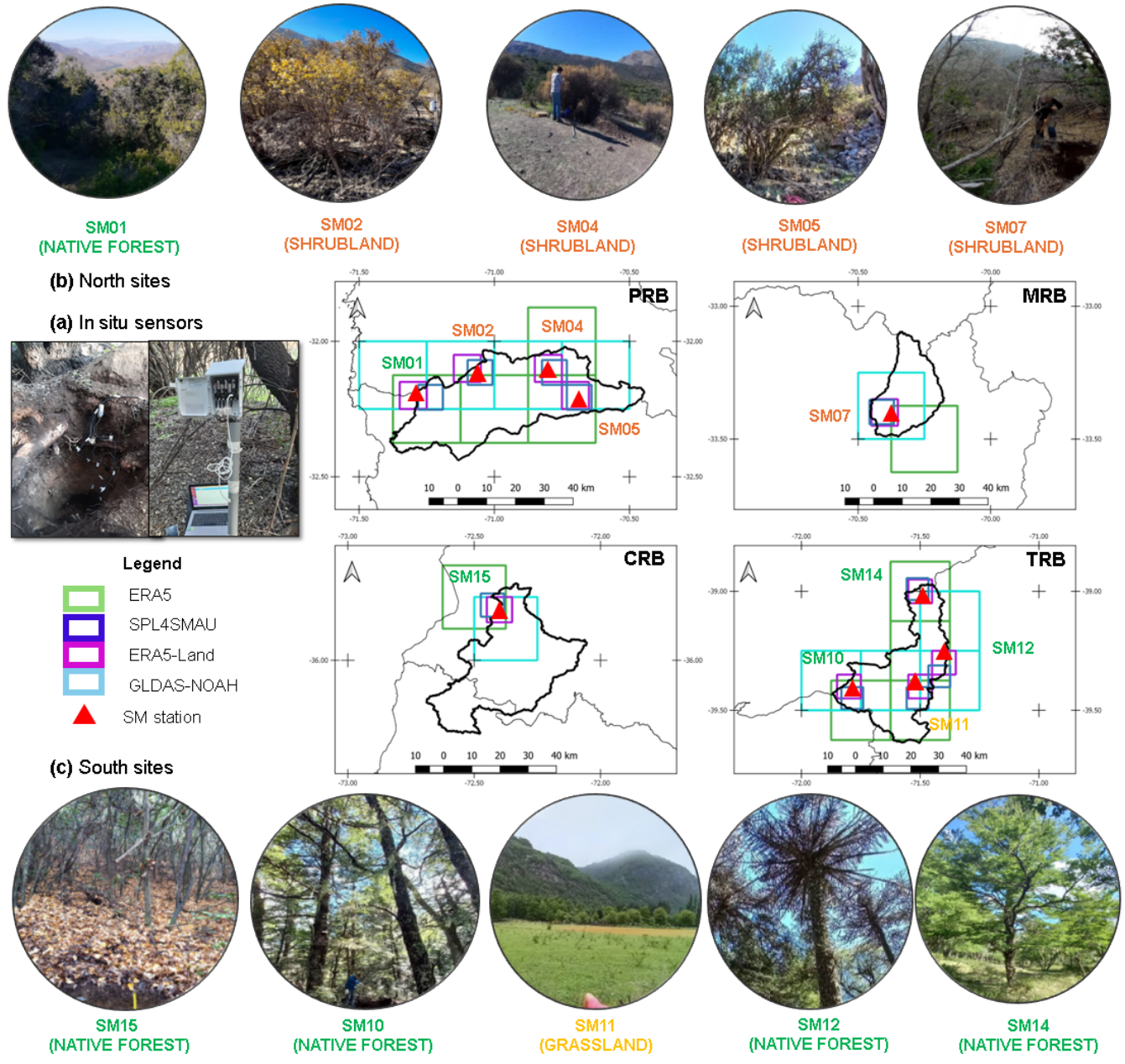

Figure 2. Locations of in situ TEROS 10 and TEROS 12 sensors. (a) Example of TEROS 10 and TEROS 12 sensors installed across various land cover types; (b) northern arid sites in the Petorca (PRB) and Mapocho (MRB) river basins; and (c) southern humid sites in the Cauquenes (CRB) and Trancura (TRB) river basins. Red triangles indicate the locations of in situ SM monitoring sites. Grid cell boundaries of each gridded SM product are shown for ERA5 (green), ERA5-Land (purple), SPL4SMAU (blue), and GLDAS-Noah (lightblue).

https://doi.org/10.5194/egusphere-2025-2606
Preprint. Discussion started: 28 July 2025

Table 2. Summary of in situ SM sensors and main characteristics of each monitoring site

n	ID	Catchment	Sector	Landcover	Latitude (°)	Longitude (°)	Elev. (m a.s.l.)	Slope (%)	AI (P/PET)	Sensor depth [cm]
1	SM01	PRB	North	Native Forest	-32.22	-71.28	574	20.7	0.17	10, 30, 50, 80, 130
2	SM02	PRB	North	Shrubland	-32.14	-71.05	879	4.2	0.14	10, 30, 50, 80, 120
3	SM04	PRB	North	Shrubland	-32.07	-70.82	1386	18.7	0.14	10, 40, 80, 110*
4	SM05	PRB	North	Shrubland	-32.22	-70.70	1240	22.8	0.15	10, 40, 70, 115*
5	SM07	MRB	North	Shrubland	-33.40	-70.37	1341	27.5	0.32	10, 30, 60, 100, 140*
6	SM15	CRB	South	Native Forest	-35.82	-72.40	613	14.6	0.72	10, 40, 70, 120*, 170*
7	SM10	TRB	South	Native Forest	-39.43	-71.78	861	11.9	1.59	10, 30, 70, 120*, 160*, 200*
8	SM11	TRB	South	Grassland	-39.40	-71.54	401	1.3	1.39	10, 30, 60, 110*
9	SM12	TRB	South	Native Forest	-39.28	-71.56	850	5.9	0.97	10, 30, 60, 100, 150*, 200*
10	SM14	TRB	South	Native Forest	-39.02	-71.47	1041	24.5	1.20	10, 30, 50, 115*

PRB: Petorca River Basin, MRB: Mapocho River Basin, CRB: Cauquenes River Basin, TRB: Trancura River Basin. *The sensors at these depths were not used in the present study. AI: Aridity index.

Table 3. Soil texture for each in situ monitoring site for SSM (0–5 cm) and RZSM (0–100 cm).

n	**ID**	**Dominant species**	**ChSPD**	**SSM (0–5 cm)**		**RZSM (0–100 cm)**		
				Clay (%)	Sand (%)	Silt (%)	Clay (%)	Sand (%)	Silt (%)
1	SM01	Cryptocarya alba	13640	19.84	59.40	20.75	23.19	58.41	18.40
2	SM02	Colliguaja odorifera	13641	13.12	63.06	23.82	19.14	62.02	18.84
3	SM04	Retanilla trinervia	13910	19.41	54.86	25.72	20.95	55.23	23.82
4	SM05	Porlieria chilensis	13911	13.56	55.32	31.12	15.83	54.21	29.96
5	SM07	Lithraea caustica	13644	14.97	59.84	25.19	15.16	59.11	25.73
6	SM15	Nothofagus glauca	13667	15.57	67.16	17.27	19.14	65.43	15.44
7	SM10	Nothofagus dombeyi	13927	8.62	62.80	28.58	7.67	64.14	28.18
8	SM11	Ruderal grassland	13928	6.83	69.20	23.97	7.50	70.09	22.41
9	SM12	Araucaria araucana	13929	9.83	60.38	29.78	8.41	61.57	30.02
10	SM14	Nothofagus antarctica	13931	6.11	63.61	30.28	5.81	65.78	28.41

Clay, silt, and sand percentages are obtained from CLSoilMaps (Dinamarca et al., 2023), which provides data for the following layers: 0–5, 5–15, 15–30, 30–60, 60–100, and 100–200 cm. In addition, the corresponding ChSPD code (Seguel et al., 2024) is shown for each site, referencing the original database of 14,029 soil profile descriptions across Chile. Detailed descriptions of the specific profiles used in this study are available in supplementary material S1 (Zambrano-Bigiarini et al., 2025).

https://doi.org/10.5194/egusphere-2025-2606
Preprint. Discussion started: 28 July 2025

3 Methodology

3.1 Data processing

3.1.1 Common temporal resolution

All gridded SM data were downloaded at their highest temporal resolution, and time series were extracted at the grid cell corresponding to each in situ monitoring site. As GLDAS-Noah and SPL4SMAU provide data at 3-hour intervals, all analyses were conducted at this common temporal resolution. To ensure temporal consistency, hourly data from ERA5, ERA5-Land, and in situ measurements were averaged into 3-hour intervals starting at 00:00:00 UTC.

3.1.2 Surface soil moisture

Table 2 shows that all upper in situ SM measurements were taken at 10 cm depth and, therefore, this depth was adopted as representative of in situ SSM. On the other hand, each gridded dataset defines SSM over different soil depths and, therefore, a single definition of SSM was adopted to ensure a fair comparison between all SM datasets and in situ observations. For ERA5 and ERA5-Land, the top layer of 0–7 cm was selected to represent SSM, as it is closest to the surface conditions measured by in situ sensors. On the other hand, GLDAS-Noah defines SSM as the 0–10 cm layer, and SMAP SPL4SMAU provides direct SSM estimates for the 0–5 cm layer, which are very close to the in situ sensor depth and require no additional adjustments.

3.1.3 Root zone soil moisture

Table 1 shows the different number of soil layers used all gridded datasets to estimate the SM dynamics in the root zone of the soil profile. In particular, ERA5 and ERA5-Land provide SM estimates for four layers up to 289 cm depth. GLDAS-Noah also provides SM estimates for four layers, but up to 200 cm; and SPL4SMAU provides only a single RZSM estimate from 0 to 100 cm depth. Therefore, in this work, the root zone considered for analysing SM dynamics was defined from 0 to 100 cm depth, as this was the only depth for which all gridded datasets have information. Consequently, the RZSM for all gridded datasets, except SPL4SMAU, was computed as a weighted average of the soil water content of the top three soil layers (0–100 cm), as shown in Figure 3a) and described in Equation 1a.

On the other hand, each in situ monitoring site has a different number of SM sensors, each located at a different depth (see Table 2). Therefore, in order to be compared against the gridded RZSM, a single estimate of RZSM was calculated for each site, using a weighted average of all in situ measurements to the depth closest to 100 cm, following Xing et al. (2021), as shown in Figure 3b) and described in Equation 1b and Equation 2.

$$\theta_{RZSM}^{GD} = \frac{1}{100}\sum_{i=1}^{i=n}\theta_i \cdot t_i \quad (1a) \qquad \theta_{RZSM}^{IS} = \frac{1}{100}\sum_{i=1}^{i=n}\theta_i \cdot e_i \quad (1b)$$

https://doi.org/10.5194/egusphere-2025-2606
Preprint. Discussion started: 28 July 2025

$$e_i = H_i - H_{i-1} \quad \text{(2a)} \qquad H_i = d_i + \frac{d_{i+1} - d_i}{2} \quad \text{(2b)} \qquad H_1 = e_1 = 2 \cdot d_1 \quad \text{(2c)}$$

In Figure 3 and equations 1 and 2, θ_i represents the volumetric soil moisture, [m^3/m^3], at the i-th soil layer; t_i and e_i are the thickness of the i-th soil layer in the gridded SM dataset and in situ monitoring site, respectively; d_i is the depth of the i-th in situ SM sensor; h_1, h_2, h_3 are the depths of to bottom of each gridded soil layer; and $H_1, ..., H_n$ are the depths of to bottom of the i-th soil layer associated to the in situ θ_i. This method provides a representative estimate of RZSM by integrating data from multiple depths to capture variability across the soil profile.

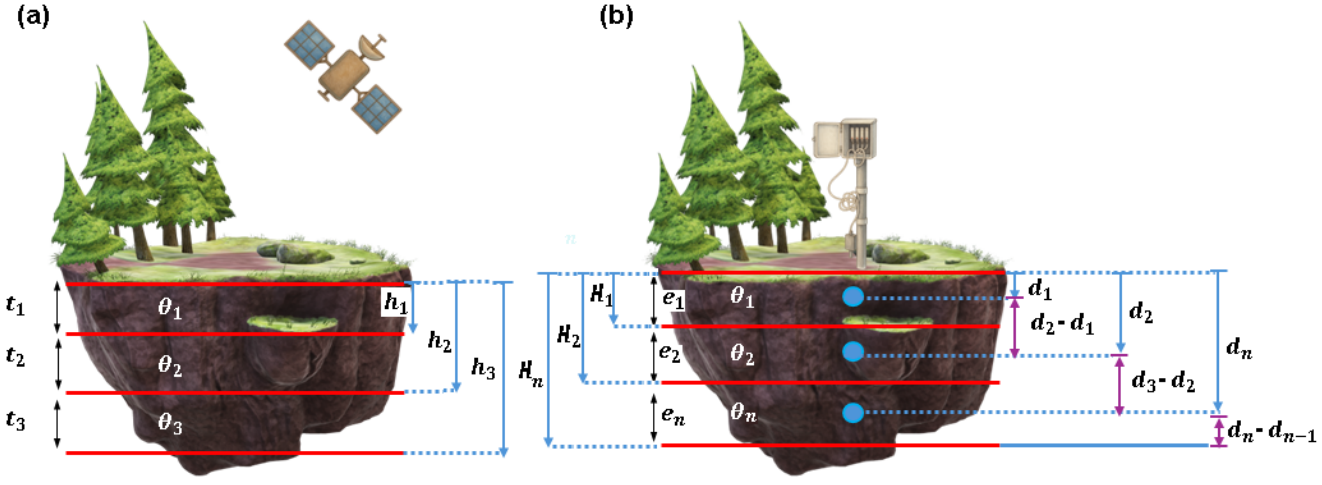

Figure 3. Panel a) illustrates the computation of the RZSM for all gridded datasets, except SPL4SMAU, using the first three soil layers of each SM product. Panel b) illustrates the computation of the RZSM for each in situ monitoring site, using n SM sensors installed at depths$d_1, ..., d_n$.

3.2 Evaluation of gridded SM datasets

The evaluation of the gridded SM datasets involved the application of two different methods: i) a traditional time series comparison of gridded SM estimates with in situ observations using statistical metrics of performance, and ii) a comparison of SM signatures to assess important aspects of SM dynamics at each site. The following sections provide a detailed description of both methods.

https://doi.org/10.5194/egusphere-2025-2606
Preprint. Discussion started: 28 July 2025

3.2.1 Statistical metrics of performance

To evaluate the gridded SM estimates against in situ observations we first used four well-known statistical metrics: i) the unbiased root mean square error ($ubRMSE$; Entekhabi et al., 2014), ii) the percent bias ($PBIAS$; Yapo et al., 1996), iii) the Spearman rank correlation coefficient (ρ), and iv) the modified Kling-Gupta efficiency (KGE'; Kling et al., 2012). ubRMSE removes the mean bias in traditional RMSE caused by differences in spatial representativeness between in situ SM measurements and gridded datasets, making it a more reliable metric for evaluating deviations from in situ observations (Entekhabi et al., 2014). A lower ubRMSE indicates superior model performance. PBIAS quantifies the systematic overestimation or underestimation of the gridded dataset (Yapo et al., 1996), with values equal to zero indicating unbiased representation of in situ values, and positive (negative) values indicate overestimation (underestimation). The Spearman rank correlation coefficient (ρ), unlike its Pearson counterpart, evaluates the strength and direction of a monotonic relationship between gridded and observed values. As a non-parametric metric, it is less affected by outliers or deviations from normality (Helsel and Hirsch, 1993), making it particularly suitable for SM time series with non-linear dynamics (Wang et al., 2021). In this study, ρ was calculated using deseasonalised time series, where each value is adjusted by subtracting the monthly mean SM value, to remove the seasonal component and ensure a consistent evaluation of temporal variability. This approach follows the general framework proposed by Albergel et al. (2012) to account for seasonal influences when evaluating SM time series, but instead of applying a centred 35-day moving average window, we used the long-term monthly mean for each calendar month as seasonal reference. The modified KGE' combines the Pearson correlation, bias, and variability into a single metric to provide a comprehensive view of performance (Kling et al., 2012). Higher KGE values, with an optimum of 1, indicate a well-performing gridded dataset, which accurately captures both the temporal dynamics and distributional characteristics of in situ SM. The four selected metrics have been widely used in the evaluation of remotely-sensed SM datasets (e.g., Beck et al., 2021; Peng et al., 2021; Liu et al., 2024; Zheng et al., 2024). Detailed formulas and their interpretations are provided in Table 4, and all the computations were made with the `hydroGOF` R package (Zambrano-Bigiarini, 2024).

These metrics were calculated at a 3-hour time step to match the temporal resolution of the GLDAS-Noah and SPL4SMAU products and to allow accurate assessment of SM dynamics across different temporal scales. This temporal adjustment also takes into account the availability of in situ measurements and ERA5 products at hourly intervals. Performance thresholds, ideal values and detailed interpretations of these metrics are described in Table 4. This structured approach categorises performance from excellent to poor, facilitating a comprehensive comparison between datasets and highlighting the different capabilities of each SM product in representing the observed soil moisture dynamics.

Finally, a regional-scale assessment beyond individual point-to-pixel comparisons was carried out, where all 3-hourly in situ and gridded SM time series were aggregated separately for the northern and southern regions. For the northern region, in situ time series from SM02, SM04, SM05, SM01, and SM07 were averaged to create a single representative time series, while for the southern region, the same was made for SM15, SM12, SM14, SM11, and SM10. These two regional in situ averages were then compared to the corresponding gridded averages, which were obtained by averaging all grid cells from each SM product located within the northern (PRB, MRB) and southern (SRB, TRB) catchments, respectively.

https://doi.org/10.5194/egusphere-2025-2606
Preprint. Discussion started: 28 July 2025

Table 4. Performance metrics, including formulas, ranges of variation, ideal values, and interpretation criteria.

Metric	Formula	Range of variation	Ideal value	Interpretation criteria
ubRMSE	$\sqrt{\frac{1}{N}\sum_{i=1}^{N}(GP_i - IS_i - \text{Bias})^2}$	$[0, +\infty[$	0	E < 0.04 ; G > 0.04; S > 0.08 ; B > 0.12
PBIAS	$\frac{1}{N}\sum_{i=1}^{N}(GP_i - IS_i)$	$]-\infty, +\infty[$	0	E $< \lvert 10\% \rvert$; G $< \lvert 20\% \rvert$ S $< \lvert 30\% \rvert$; B $\geq \lvert 30\% \rvert$
ρ	$1 - \frac{6\sum_{i=1}^{N} d_i^2}{N(N^2-1)}$	$[-1, 1]$	1	E ≥ 0.75 ; G ≥ 0.65 S ≥ 0.5 ; B < 0.5
KGE	$1 - \sqrt{(r-1)^2 + \left(\frac{\text{CV}_{GP}}{\text{CV}_{IS}} - 1\right)^2 + \left(\frac{\overline{IS}}{\overline{GP}} - 1\right)^2}$	$]-\infty, 1]$	1	E ≥ 0.7 ; G ≥ 0.3 S $\geq$ -0.4 ; B $<$ -0.4

GP: gridded product; IS: in situ observation; CV, Coefficient of variation, E: Excellent; G: Good; S: Satisfactory; B: Bad

3.2.2 Soil moisture signatures

In addition to the standard statistical metrics, we used two SM signatures to provide a comprehensive evaluation of the gridded products. SM signatures provide a process-oriented approach to evaluate SM dynamics and capture the SM response to P events that are often overlooked by statistical metrics of performance (Branger and McMillan, 2020; Araki et al., 2022). In particular, they characterise processes such as infiltration and water retention, which are important for understanding the mechanisms of runoff generation and water storage capacity in different ecosystems (Liang et al., 2011; Tian et al., 2019).

We adapted the methodology proposed by Branger and McMillan (2020) and Araki et al. (2022) to calculate two key SM signatures: *rising time* (RT) and *amplitude* (A). RT represents the time delay between the onset of a P event and the maximum of the SM, and reflects the response time of the soil. On the other hand, A represents the change in SM during the precipitation event, which is calculated as the difference between the maximum SM value and its initial state. Figure 4 shows a conceptual representation of the two SM signatures used in this study, and illustrates how RT and A capture the timing and magnitude of SM responses to different P events.

https://doi.org/10.5194/egusphere-2025-2606
Preprint. Discussion started: 28 July 2025

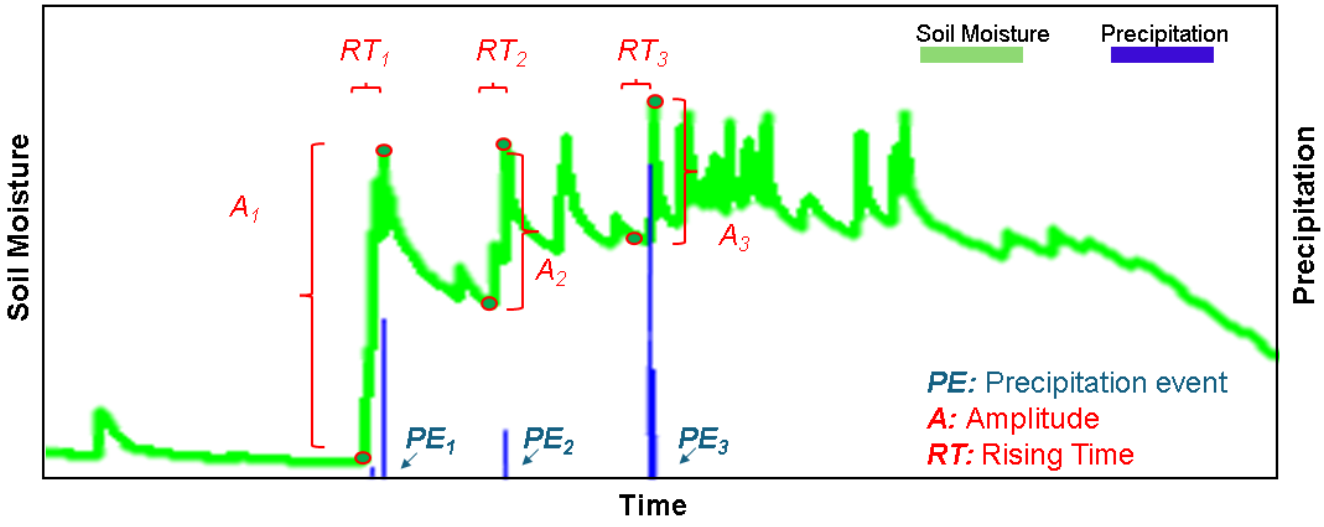

Figure 4. Soil moisture signatures: rising time (RT) and amplitude (A) for selected precipitation events (PE).

To assess the sensitivity of SM dynamics to different combinations of P characteristics and antecedent SM conditions, for each site we analysed two precipitation events, considered as extreme cases of the wide range of P and SM combinations that a site experiences during a year: i) the *first precipitation event* of the year (FE), i.e., when the SM is at its driest condition; and ii) the *most intense precipitation event* within the wet season of the year (IE), when the SM should be close to field capacity. Precipitation events were identified using the criteria described in Section 3.2.3 to ensure consistency between sites and datasets.

3.2.3 Identification of precipitation events

To identify individual P events (PEs) for the SM signature analysis at each site, we used hourly P data from 1 January 2022 to 31 December 2023, recorded by the rain gauge nearest to each in situ SM monitoring site. The identification method, illustrated in Figure 5, follows the approach of Dunkerley (2019) and Araki et al. (2022). A P event is defined as any period with an intensity larger or equal to 0.2 mm h^{-1}, separated from other events by at least six consecutive dry hours (i.e., hours with less than 0.2 mm of P). The end of a P event is defined as when a new P event began or five days after the last recorded P amount. This five-day buffer after the last recorded P amount is important to clearly distinguish individual storms, as it helps to avoid biases due to evapotranspiration effects that could otherwise influence the SM response (Araki et al., 2022). The adopted identification framework ensures that SM signatures associated with storm events are accurately captured and provides a robust and complementary basis for assessing SM dynamics in response to P events.

https://doi.org/10.5194/egusphere-2025-2606
Preprint. Discussion started: 28 July 2025

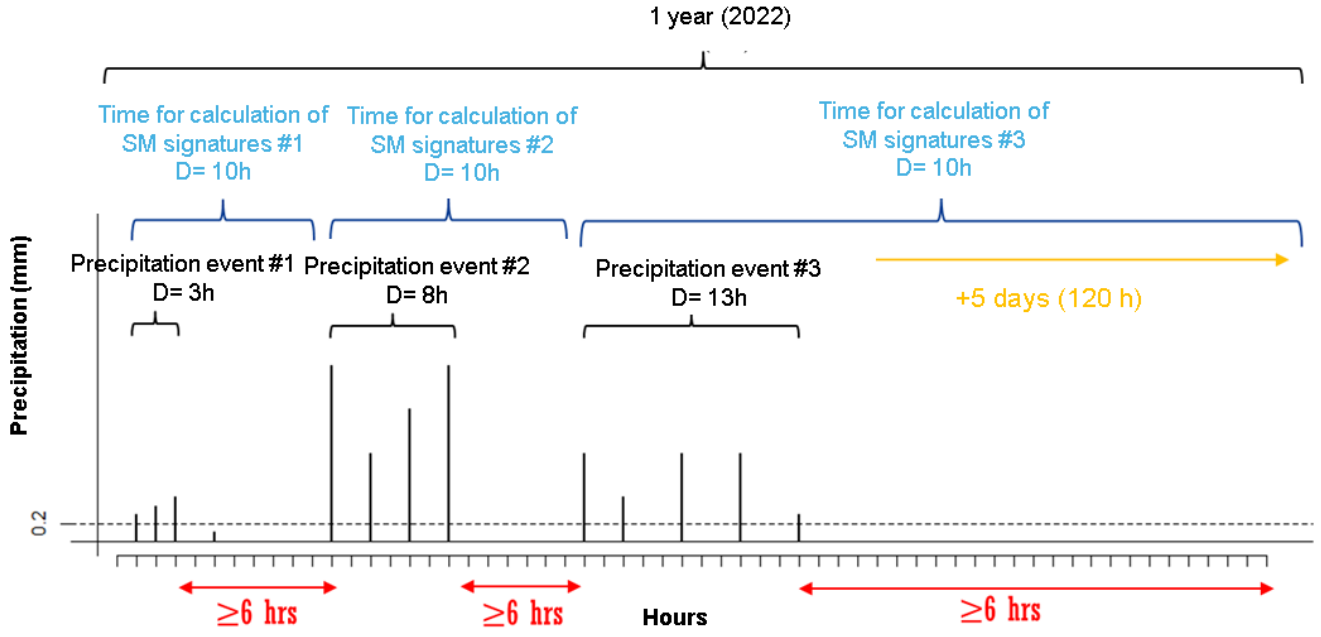

Figure 5. Selection of P events and their corresponding SM signature computation periods. Each storm event is separated by dry intervals of at least six hours, and the SM signature computations extend beyond the P event itself, with a five-day buffer period to ensure proper distinction between successive P events.

4 Results and discussion

4.1 Overall soil moisture dynamics

Figures 6 and 7 show the temporal dynamics of SSM, RZSM and P for four monitoring sites that are representative of the arid shrublands that predominate in the north (SM05 and SM07) and the humid native forests in the south (SM15 and SM14), respectively. They show a distinct event-driven SM response that emphasises different SM responses to P events. The remaining time series are available in Supplementary Material S2 (Zambrano-Bigiarini et al., 2025).

Figure 6 shows that at SM05 (PRB, panels a-c), both in situ SSM and RZSM remained consistently low during the dry season (January to May), with average values close to 0.1 m^3/m^3. The first P event of 2022 (01-Jun 21:00 hrs – 03-Jun 18:00 hrs; 3.4 mm total) had no noticeable impact on either SSM or RZSM. A sharp increase in August 2022 corresponded to the soil response to an intense P event (19.2 mm in 21 hours), with SSM and RZSM reaching values of 0.34 and 0.27 m^3/m^3, respectively. On the other hand, all gridded SM products exhibited an important variability in SSM during the dry season, which contrasts with the relatively flat response observed in the in situ measurements. While this variability was largely dampened in the root zone, all products still overestimated RZSM. During the most intense P event of the year, GLDAS-Noah closely followed in situ SSM and RZSM, while ERA5 and ERA5-Land overestimated it (particularly during the recession curve) and SMAP SPL4SMAU underestimated it. At SM07 (MRB, panels d-f), the overall behaviour of both in situ and gridded SSM and RZSM was similar to

https://doi.org/10.5194/egusphere-2025-2606
Preprint. Discussion started: 28 July 2025

that observed at SM05. However, SMAP SPL4SMAU showed a much closer agreement with the in situ SSM. It is noteworthy that in September 2022, while in situ RZSM was decreasing at both sites, ERA5 and ERA5-Land showed some increases. This discrepancy suggests that the P data used in these gridded products exhibit a substantial difference in time from the in situ
300 observations.

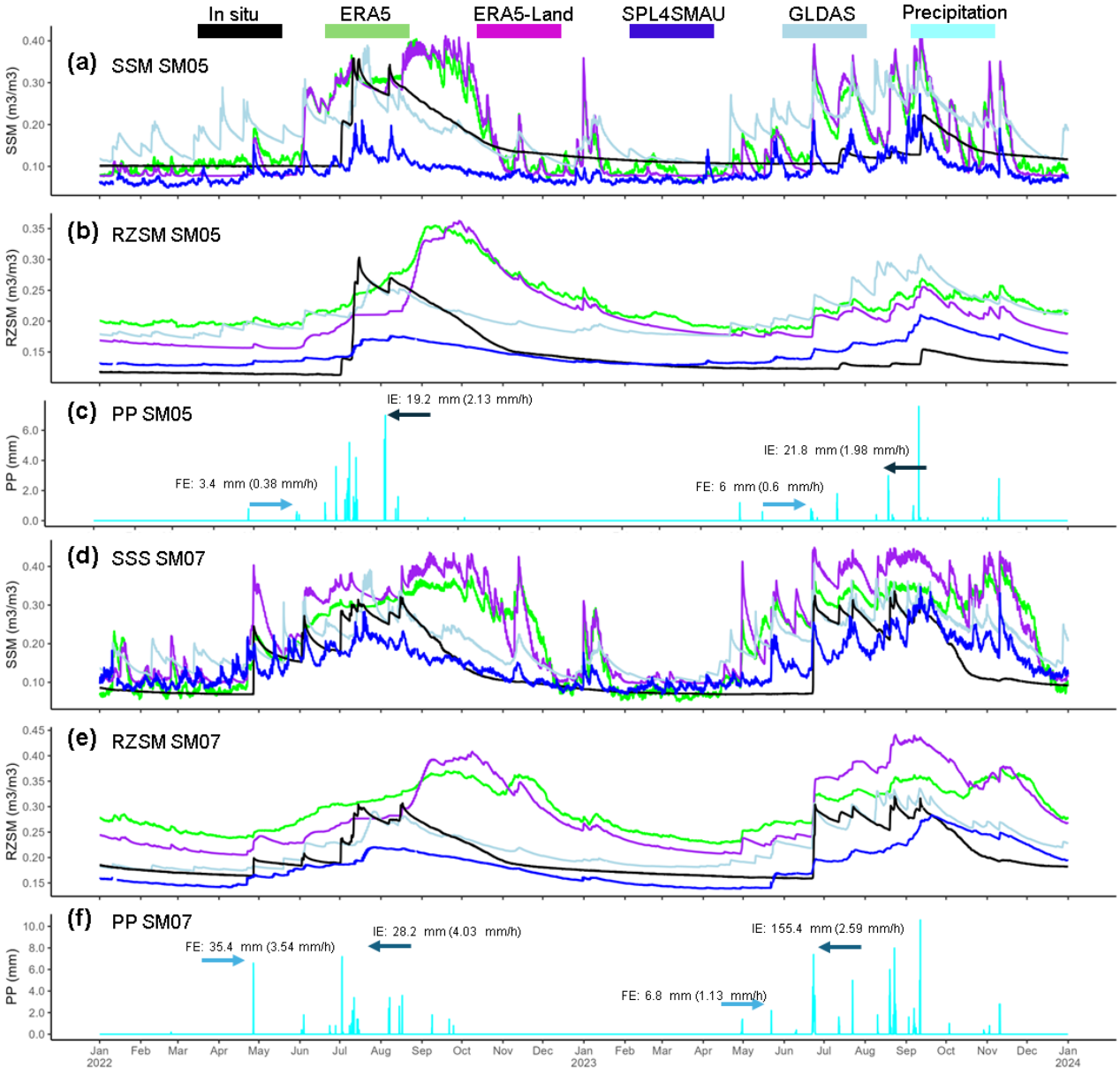

Figure 6. Panels (a), (b), and (c) show time series of surface soil moisture (SSM), root zone soil moisture (RZSM), and precipitation (P), respectively, for 2022–2023 at site SM05 (shrubland in PRB). Panels (d), (e), and (f) present the same variables for site SM07 (shrubland in MRB). The labels FE and IE indicate the first and the most intense precipitation event of the year, respectively.

https://doi.org/10.5194/egusphere-2025-2606
Preprint. Discussion started: 28 July 2025

Figure 7 shows that at SM15 (CRB, panels a–c), both in situ SSM and RZSM presented a gradual decline in SM during the dry season (Oct-Mar), reaching average values of 0.16 m^3/m^3 for both SSM and RZSM, which is much higher than the value observed at the northern sites, especially for SSM. After the first P event of the year (26-Apr 18:00 hrs to 27-Apr 12:00 hrs; 6.4 mm total), an important increase in in situ SM was observed, which had a greater impact on SSM than on RZSM. During the rainy season (Apr-Sep), both SSM and RZSM showed high variability in their response to P events, with average values of about 0.35 and 0.30 m^3/m^3, respectively. On the other hand, all gridded products captured well the seasonal patterns in both soil layers. ERA5-Land most closely matched the timing and magnitude of the in situ observations, while ERA5 and GLDAS-Noah tend to underestimate soil water content, and SMAP SPL4SMAU slightly overestimated it. During the dry season, the underestimation of SM by ERA5 and GLDAS-Noah was about 0.10 m^3/m^3. At SM14 (TRB, panels d–f), the frequency and intensity of P events were higher than in SM15. This led to greater variability and higher mean values of both the in situ SSM and the RZSM, including several P events during the dry season (Oct-Mar). All gridded SSM products captured the temporal pattern of in situ observations, but consistently underestimated their magnitude. For RZSM, ERA5 and ERA5-Land overestimated soil water content, while GLDAS-Noah consistently underestimated it. SMAP SPL4SMAU underestimated RZSM during the wet season, but overestimated it during the dry season.

4.2 Statistical metrics of performance

4.2.1 Surface soil moisture

Figure 8 summarises the time series comparison of gridded products against in situ observations of SSM at all monitoring sites, using the four statistical metrics defined in Section 4.2.1. In each panel, monitoring sites are ordered from left to right following a north-south latitudinal gradient, from the most arid sites to the most humid ones, and the yellow shaded area stands for an excellent performance. Panel a) shows that most products had good (ubRMSE between 0.04 and 0.08) to excellent (ubRMSE < 0.04) performance. Errors were higher at the northern sites than in the southern ones. In the north, SPL4SMAU generally achieved the lowest ubRMSE values, ranging from 0.034 to 0.052 m^3/m^3, while the other products typically showed ubRMSE values between 0.051 and 0.080 m^3/m^3. At the southern sites, most products achieved excellent ubRMSE values (below 0.040 m^3/m^3), with ERA5 performing best at SM14 and SM15 (0.033 and 0.039 m^3/m^3, respectively). The full set of performance values for all products and stations is provided in Appendix A and in Supplementary Material S2 (Zambrano-Bigiarini et al., 2025). In particular, sites SM05 and SM07 (previously discussed in Section 4.1) exhibited good ubRMSE values for ERA5 (0.066 and 0.080 m^3/m^3, respectively) and ERA5-Land (0.077 m^3/m^3 in both sites), which was in line with the overestimations described in Section 4.1. In contrast, SPL4SMAU and GLDAS-Noah presented lower errors at SM05 and SM07, with ubRMSE values of 0.046 and 0.052 m^3/m^3 for SPL4SMAU and 0.057 and 0.049 m^3/m^3 for GLDAS-Noah, respectively. At the southern sites, in particular SM14 and SM15, most products achieved excellent ubRMSE values (below 0.040 m^3/m^3). It is worth noting that ERA5 performed best at these two southern sites, with ubRMSE values of 0.033 and 0.039 m^3/m^3 for SM14 and SM15, respectively. Panel b) shows that all northern arid sites exhibited PBIAS values above 25% for ERA5, ERA5-Land and GLDAS, while SMAP SPL4SMAU presented PBIAS lower than -25% in most monitoring sites. In the humid south, most

https://doi.org/10.5194/egusphere-2025-2606
Preprint. Discussion started: 28 July 2025

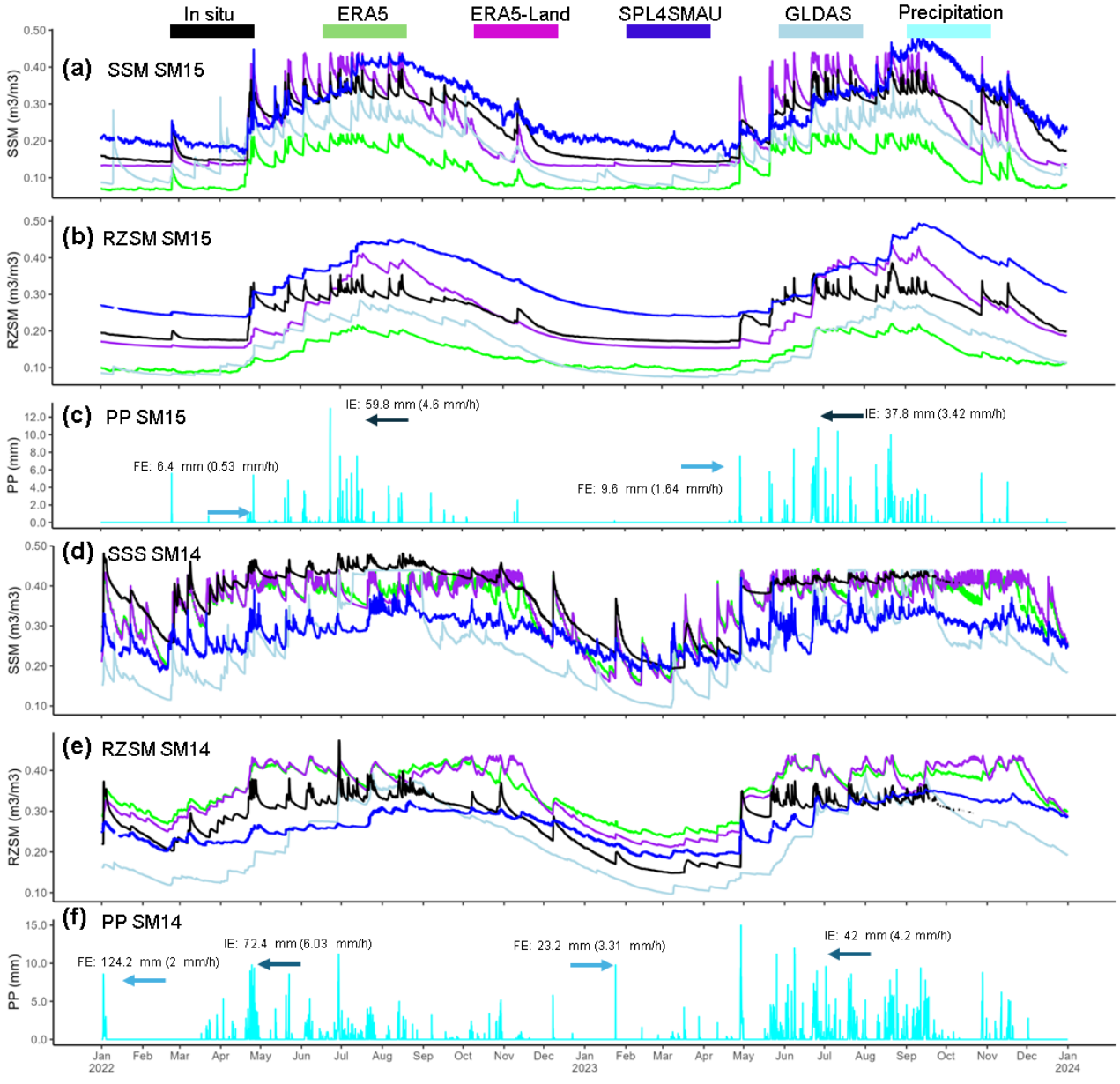

Figure 7. Panels (a), (b), and (c) show time series of surface soil moisture (SSM), root zone soil moisture (RZSM), and precipitation (P), respectively, for 2022–2023 at site SM15 (native forest in the CRB). Panels (d), (e), and (f) present the same variables for site SM14 (native forest in the TRB). The labels FE and IE indicate the first and the most intense precipitation event of the year, respectively.

products showed PBIAS values below 25%, except in SM11 and SM10. Panel c) shows that in the northern sites, the Spearman rank correlations (ρ) between deseasonalised time series were lower than 0.5 for all gridded products, with GLDAS-Noah showing negative values in all arid monitoring sites but SM07. The ρ values showed an important increase in the humid south,

https://doi.org/10.5194/egusphere-2025-2606
Preprint. Discussion started: 28 July 2025

with ERA5 and ERA5-Land reaching values above 0.75 for all gridded products and monitoring sites but SM11. Finally, panel d) shows good KGE values in al northern sites ($KGE \leq 0.3$) but SM02, and higher values in most humid southern sites.

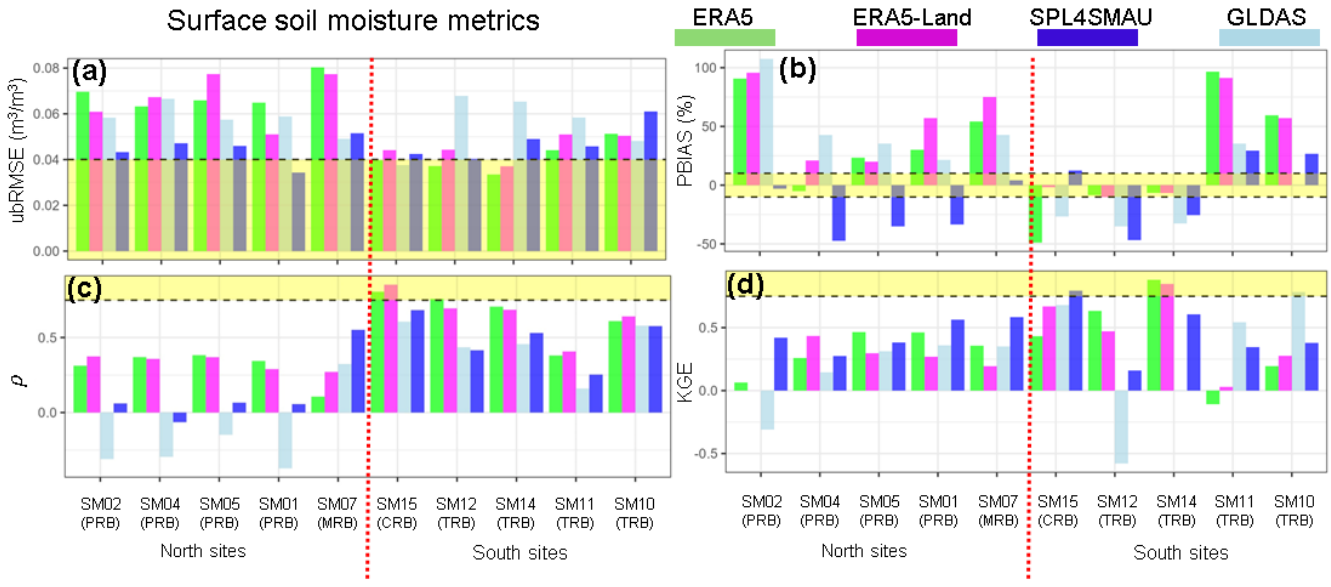

Figure 8. Panels a), b), c) and d) shows the ubRMSE, PBIAS, ρ and KGE performance metrics obtained for SSM at each in situ monitoring site, respectively. The in situ monitoring sites are shown on the x-axis, from the most arid (left) to the most humid (right) ones. The yellow shaded area indicate an excellent performance range based on Table 4. The colours represent the data sources: green for ERA5, pink for ERA5-Land, blue for SPL4SMAU, and light blue for GLDAS-Noah.

SPL4SMAU generally aligned well with in situ SSM measurements across northern monitoring sites, as evidenced by low ubRMSE values and relatively high KGE′ scores (Figure 8). These findings are consistent with previous studies that highlight the robustness of SPL4SMAU in arid and semi-arid regions (Reichle et al., 2017a, b; Xu, 2020; Zheng et al., 2024). Notably, SPL4SMAU showed stable behaviour during dry periods, avoiding the spurious SSM peaks seen in other gridded products. For instance, during December 2022, SPL4SMAU closely tracked observed SSM, while other datasets recorded abrupt increases not supported by ground observations. A similar, though slightly weaker, performance was observed at SM05. However, the deseasonalised Spearman rank correlation (ρ) revealed poor to very poor performance for both GLDAS-Noah and SPL4SMAU at most sites, with the exception of SM07 (Mapocho River Basin), a transitional arid ecosystem that recorded the highest KGE′ among northern stations and reliably captured dry-season dynamics (Figure 6).

ERA5 and ERA5-Land showed stronger performance in humid southern sites (Figure 7), particularly SM14 and SM15, where they achieved excellent ubRMSE values (< 0.040 m^3/m^3) and high Spearman correlations ($\rho > 0.75$), indicating good agreement with in situ SSM. The good performance of ERA5 in humid environments is likely due to the assimilation of surface variables such as air temperature and humidity, which allows for more realistic lower boundary conditions and, consequently, improves the accuracy of RZSM estimations in humid climates (Liu et al., 2024). On the other hand, the good correlation

https://doi.org/10.5194/egusphere-2025-2606
Preprint. Discussion started: 28 July 2025

of ERA5-Land retrievals with empirical measurements in humid environments, where soil moisture plays a crucial role in influencing evapotranspiration and local climate patterns, confirms previous findings by Schönauer et al. (2024); Zheng et al. (2024). These results confirm the capability of ERA5 and ERA5-Land in capturing SSM dynamics in humid regions, supporting their use for long-term hydrological monitoring in those regions (Lal et al., 2022; Wu et al., 2021).

However, in arid northern sites, their performance declined, with higher ubRMSE and PBIAS values and lower deseasonalised correlations ($\rho < 0.5$), reflecting limitations under dry conditions. This limited capability of ERA5 and ERA5-Land to effectively capture soil moisture dynamics in arid environments has been already documented in the literature (Chang et al., 2020; Ling et al., 2021; Andaryani et al., 2021; Jiao et al., 2024). Their coarse spatial resolution and oversimplified representation of land-atmosphere interactions is not able to incorporate local climatic and geological conditions adequately (Ling et al., 2021). This, limits their ability to represent rapid evaporation processes characteristic of dry regions, which are significantly underestimated by reanalysis products (Chang et al., 2020; Jiao et al., 2024). These deficiencies often result in biased soil moisture estimates, particularly under high evaporative demand and limited precipitation conditions (Jiao et al., 2024). Additionally, these reanalysis products show reduced sensitivity to extreme climatic events—such as prolonged droughts—and may lag in responding to abrupt meteorological changes, further compromising their reliability in arid environments (Andaryani et al., 2021). To enhance their performance, incorporating local observations and integrating additional atmospheric datasets sensitive to soil moisture variability has been recommended in literature to avoid low performances in ecohydrologically complex and under-monitored arid regions (e.g. Sanchez-Mejia and Papuga, 2017; Sehgal et al., 2017; Senanayake et al., 2022).

4.2.2 Root zone soil moisture

Figure 9, analogous to Figure 8, summarises the evaluation metrics for RZSM. Panel a) shows that most products performed well in terms of ubRMSE, with excellent (ubRMSE < 0.04) or good (0.04 $\leq$ ubRMSE < 0.08) match with in situ observations across sites. ERA5-Land performed best in the arid northern sites, while ERA5 achieved the highest performance in the humid southern regions. In contrast, GLDAS-Noah overestimated RZSM across most locations. Panel b) indicates that humid southern sites generally had lower PBIAS values than the northern sites. SPL4SMAU showed the lowest PBIAS at most sites, while GLDAS-Noah underestimated in situ values in the south. ERA5 and ERA5-Land presented PBIAS values close to or larger than 50% in al northern sites but SM04; however, this bias decreased to less than 25% in the south. Panel c) shows a general better agreement between deseasonalised time series in the southern sites compared to the northern ones, in terms of the Spearman rank correlations (ρ). ERA5 and ERA5-Land achieved good to excellent correlations ($\rho > 0.65$ and $\rho > 0.75$, respectively) in most sites, whereas GLDAS-Noah and SPL4SMAU often led to negative ρ values in northern sites. Finally, panel d) shows that most of the products had higher KGE' values at the humid sites in the south than in the arid north. ERA5 and ERA5-Land achieved good KGE values (> 0.3) and the best overall performance at all sites except SM02, while GLDAS-Noah performed the worst, even with negative KGE' values at two southern sites (SM12 and SM14).

https://doi.org/10.5194/egusphere-2025-2606
Preprint. Discussion started: 28 July 2025

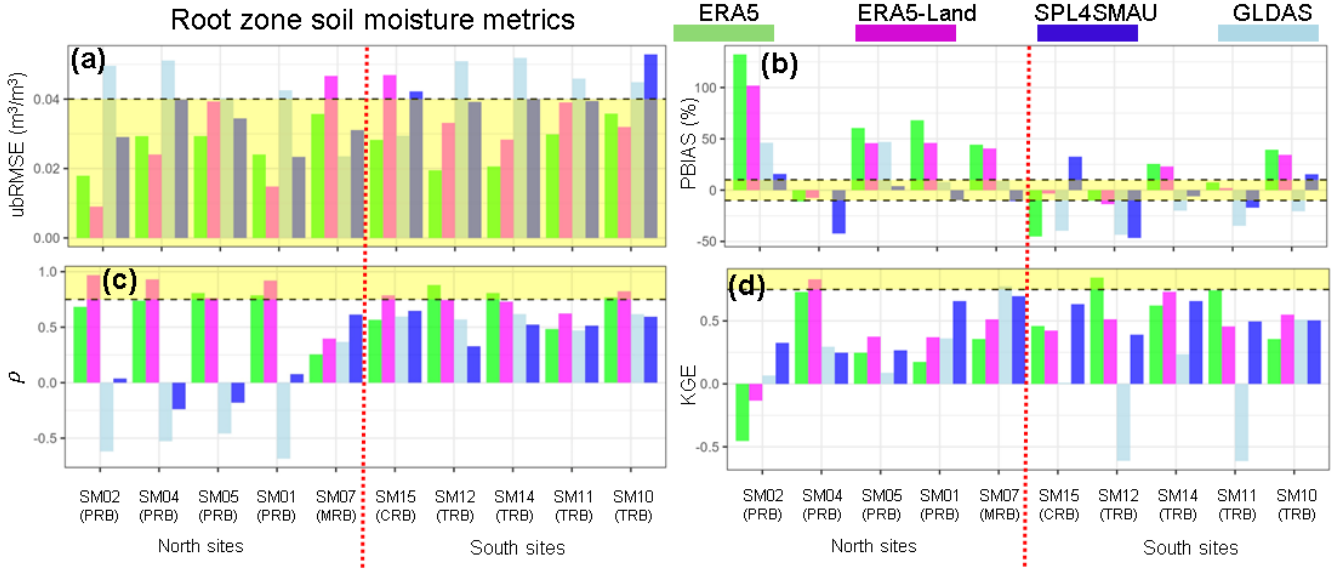

Figure 9. Panels a), b), c) and d) shows the ubRMSE, PBIAS, ρ and KGE performance metrics obtained for RZSM at each in situ monitoring site, respectively. The in situ monitoring sites are shown on the x-axis, from the most arid (left) to the most humid (right) ones. The yellow shaded area indicate an excellent performance range based on Table 4. The colours represent the data sources: green for ERA5, pink for ERA5-Land, blue for SPL4SMAU, and light blue for GLDAS-Noah.

In general, gridded products performed better for RZSM than for SSM, with higher KGE′ values and lower errors across most sites. An exception was observed at SM05, where all products performed better for SSM than for RZSM. This may be explained by the local soil profile—sandy loam with high gravel content and minimal clay—conditions known to limit water retention in deeper layers and complicate RZSM representation in land surface models (Al-Yahyai et al., 2006; Beck-Broichsitter et al., 2023). ERA5 and ERA5-Land showed strong performance in representing RZSM, with high Spearman correlations ($\rho > 0.65$ and $\rho > 0.75$, respectively), low ubRMSE, and good KGE′ values across most sites, particularly in the humid southern regions. These findings support the applicability of ERA5 and ERA5-Land in ecohydrological studies requiring accurate root-zone estimates (Balocchi et al., 2023).

SPL4SMAU exhibited weak Spearman correlations in southern humid sites but showed a mixed performance in the northern arid regions. At SM07 (Mapocho River Basin), SPL4SMAU achieved $\rho = 0.55$ and $KGE' = 0.58$, suggesting reasonable skill in capturing RZSM dynamics. Conversely, at sites within the Trancura River Basin (SM01–SM05), where passive microwave retrievals are theoretically favoured by dry conditions and sparse vegetation (Xu, 2020; Nadeem et al., 2022), SPL4SMAU performed poorly. Spearman correlations ranged from 0.06 at SM01 and SM02 to 0.07 at SM05, with a negative correlation of –0.06 at SM04. GLDAS-Noah consistently underestimated both SSM and RZSM, particularly at southern humid sites during high-intensity precipitation events. This is reflected in PBIAS values below –30% (Figure 9b) and low KGE′ values across the network. Such systematic underestimation under wet conditions limits the suitability of GLDAS-Noah for monitoring SM dynamics in humid environments (Spennemann et al., 2015; Araki et al., 2023).

https://doi.org/10.5194/egusphere-2025-2606
Preprint. Discussion started: 28 July 2025

4.2.3 Summary of regional performance

Table 5 summarises the performance of gridded SM products for SSM and RZSM across northern and southern regions, based on the average values of statistical metrics of performance. For SSM, SPL4SMAU achieved the lowest ubRMSE in the north (0.037 m^3/m^3), while ERA5-Land performed best in the south (0.031 m^3/m^3). For RZSM, ERA5 achieved the lowest ubRMSE in both regions, 0.015 m^3/m^3 in the north and 0.024 m^3/m^3 in the south, indicating a strong agreement with in situ measurements at greater depths. In terms of PBIAS, SPL4SMAU obtained relatively low percent bias values in both regions. In contrast, ERA5-Land exhibited significant overestimation in the north, with PBIAS values of 51.2% for SSM and 39.1% for RZSM. In the south, biases were more balanced across products, although GLDAS-Noah consistently underestimated SM, with PBIAS values of –20% for SSM and –30.1% for RZSM. The Spearman rank correlation coefficient (ρ) showed that ERA5 obtained the highest correlation for SSM in the north ($\rho = 0.53$), while ERA5-Land performed best for RZSM ($\rho = 0.92$). In the south, ERA5-Land achieved the highest correlations for both SSM ($\rho = 0.74$) and RZSM ($\rho = 0.75$), suggesting a strong temporal agreement with in situ measurements in humid ecosystems. In terms of the KGE', SPL4SMAU performed best for RZSM in the north ($KGE' = 0.73$), while ERA5-Land showed the highest performance in the south ($KGE' = 0.85$). Conversely, GLDAS-Noah generally had the lowest KGE′ values, particularly for RZSM in the northern catchments.

Table 5. Performance metrics for SSM (RZSM) across northern and southern regions. Metrics include ubRMSE, PBIAS, r, and KGE. Bold values indicate the best performance for each metric in the respective region.

Product	ubRMSE		PBIAS		ρ		KGE	
	North	South	North	South	North	South	North	South
ERA5	0.049 (**0.015**)	0.037 (**0.024**)	34.5 (50.6)	11.0 (9.1)	**0.53** (0.80)	0.73 (0.74)	0.56 (0.34)	0.77 (0.79)
ERA5-Land	0.051 (0.018)	**0.031** (0.025)	51.2 (39.1)	13.4 (9.2)	0.48 (**0.92**)	**0.74 (0.75)**	0.45 (0.52)	**0.83 (0.87)**
SPL4SMAU	**0.037** (0.028)	0.044 (0.044)	**-25.3 (-12.7)**	**-9.2 (-5.3)**	0.14 (-0.14)	0.54 (0.30)	**0.59 (0.53)**	0.73 (0.67)
GLDAS-Noah	0.049 (0.039)	0.039 (0.042)	45.6 (17.6)	-20.0 (-30.1)	-0.15 (-0.52)	0.47 (0.51)	0.32 (0.43)	0.47 (0.10)

4.3 Soil moisture signatures

4.3.1 Event-scale evaluation

In order to provide a closer look to the SM signatures analysed in this study, Figure 10 shows 3-hourly time series of SSM (panels a and b) and RZSM (panels c, d) recorded in 2022 at SM05, a shrubland site in the arid PRB. This figure also shows the amplitude (A) and rising time (RT) obtained during the first P event (FE) and the most intense event (IE) of the year 2022, for the in situ observations (black line) and all gridded datasets (coloured lines).

For the FE, the in situ observations showed no response in either SSM or RZSM (A = 0 m^3/m^3, RT = 0 h). In contrast, all the gridded datasets reported a soil response for this event, overestimating both in situ amplitudes and rising times. In particular, the amplitudes derived from gridded products were in [0.012, 0.116] m^3/m^3 and [0.003, 0.016] m^3/m^3 for SSM and RZSM,

https://doi.org/10.5194/egusphere-2025-2606
Preprint. Discussion started: 28 July 2025

respectively; while rising times were in [42, 45] h and [27, 45] h for SSM and RZSM, respectively. It is worth mentioning that most of the products agreed on a rising time of 42-45 h for both SSM and RZSM, except SPL4SMAU which showed a shorter RT of 27 h for RZSM.

For the most intense P event of the year, in situ measurements showed a strong SM response in both SSM and RZSM, with amplitudes of 0.066 m^3/m^3 and 0.015 m^3/m^3, respectively, and a rising times (RT) of 12 h for both layers. In contrast, all gridded datasets underestimated the amplitude and showed inconsistent rising times. For SSM, amplitudes ranged from 0.012 to 0.031 m^3/m^3, and for RZSM, from 0.004 to 0.006 m^3/m^3. On the other hand, most products underestimated RT for SSM (6–9 hours), except SPL4SMAU, which overestimated it (21 hours). For RZSM, ERA5 and ERA5-Land overestimated RT (21 hours), while SPL4SMAU and GLDAS-Noah underestimated it (9 hours each). These discrepancies highlight the challenges of accurately capturing SM dynamics during intense P events.

Figure 11 is analogous to Figure 10, but for a native forest in the southern humid TRB (SM14). In contrast to the arid SM05 site, during the FE of the year the in situ observations showed a sharp increase in both SSM and RZSM, with amplitudes of 0.185 and 0.153 m^3/m^3, respectively, and rising times of 18 h in both soil layers. Similarly, all the gridded datasets showed an important response of SSM and RZSM during this event, underestimating the amplitudes and overestimating the rising times. In particular, amplitudes derived from gridded products were in [0.007, 0.179] m^3/m^3 and [0.007, 0.063] m^3/m^3 for SSM and RZSM, respectively; while rising times were in [18, 45] h and [21, 63] h for SSM and RZSM, respectively.

For the most intense P event of the year, in situ measurements also showed an important SM response in both soil layers (though less pronounced), with amplitudes of 0.034 and 0.053 m^3/m^3, respectively, and a rising times (RT) of 12 h for both layers. For SSM, ERA5-Land had the amplitude (0.038 m^3/m^3) and rising time (RT=9 h) closest to the corresponding in situ values, followed by ERA5 ($A = 0.017$ m^3/m^3, $RT = 15$ h). For RZSM, all gridded datasets underestimated the amplitude (0.003-0.030 m^3/m^3); and most of them overestimated the rising time ($RT = 15$ h), except SPL4SMAU ($RT = 9$ h). During the most intense P event of the year, in situ measurements showed an important, but less abrupt, SM response in both layers; with amplitudes of 0.034 and 0.053 m^3/m^3 for SSM and RZSM, respectively, and rising times of 12 h in both cases. On the other hand, all the gridded datasets showed important responses in SSM and RZSM. For SSM, ERA5-Land provided the best match, with an amplitude of 0.038 m^3/m^3 and a rising time of 9 h, followed by ERA5, which reported an amplitude of 0.017 m^3/m^3 and a rising time of 15 h. For RZSM, all gridded datasets underestimated the amplitude, with values ranging from 0.003 to 0.030 m^3/m^3, and most products overestimated the rising time ($RT = 15$ h), except SPL4SMAU, which had a shorter RT of 9 h.

The evaluation of SM responses to P events offered additional insights beyond conventional statistical metrics of performance, further highlighting the regional variability identified in earlier sections. In particular, it revealed marked discrepancies between in situ observations and gridded datasets, especially across contrasting natural ecosystems.

Products such as SPL4SMAU and ERA5-Land aligned more closely with in situ SM dynamics under certain conditions; however, their performance presented large variations depending on the ecosystem type and intensity of the P event (Figures 10 and 11). This variability is illustrated by two representative sites: SM05, located in a northern shrubland, and SM14, situated in a humid native forest in the south. At SM05, the in situ sensor registered no detectable response during the first P event of

https://doi.org/10.5194/egusphere-2025-2606
Preprint. Discussion started: 28 July 2025

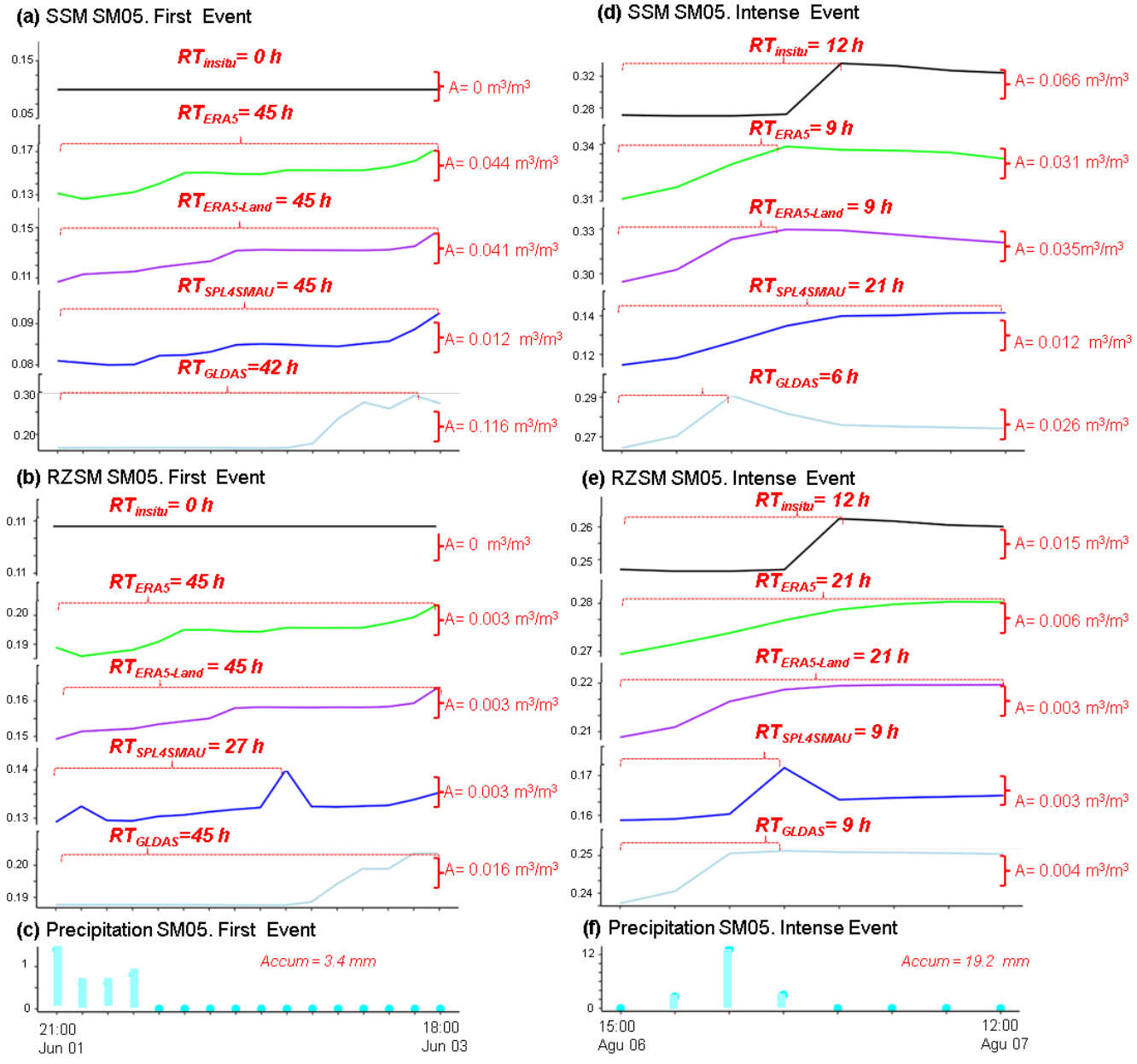

Figure 10. Amplitude (A) and rising time (RT) for the first precipitation event of 2022 in SM05 (Shrubland in Petorca). Results are shown for both surface soil moisture (SSM) and root zone soil moisture (RZSM) across observed (in situ) and gridded products. The bottom panel shows cumulative precipitation for the first event event(Accum = 3.4 mm) and Intense event (Accum = 19.2 mm) of 2022.

the year, with both the amplitude (A) and response time (RT) equal to zero. In contrast, the gridded products did simulated a response, overestimating both variables. These discrepancies highlight the challenges of capturing localised SM responses

https://doi.org/10.5194/egusphere-2025-2606
Preprint. Discussion started: 28 July 2025

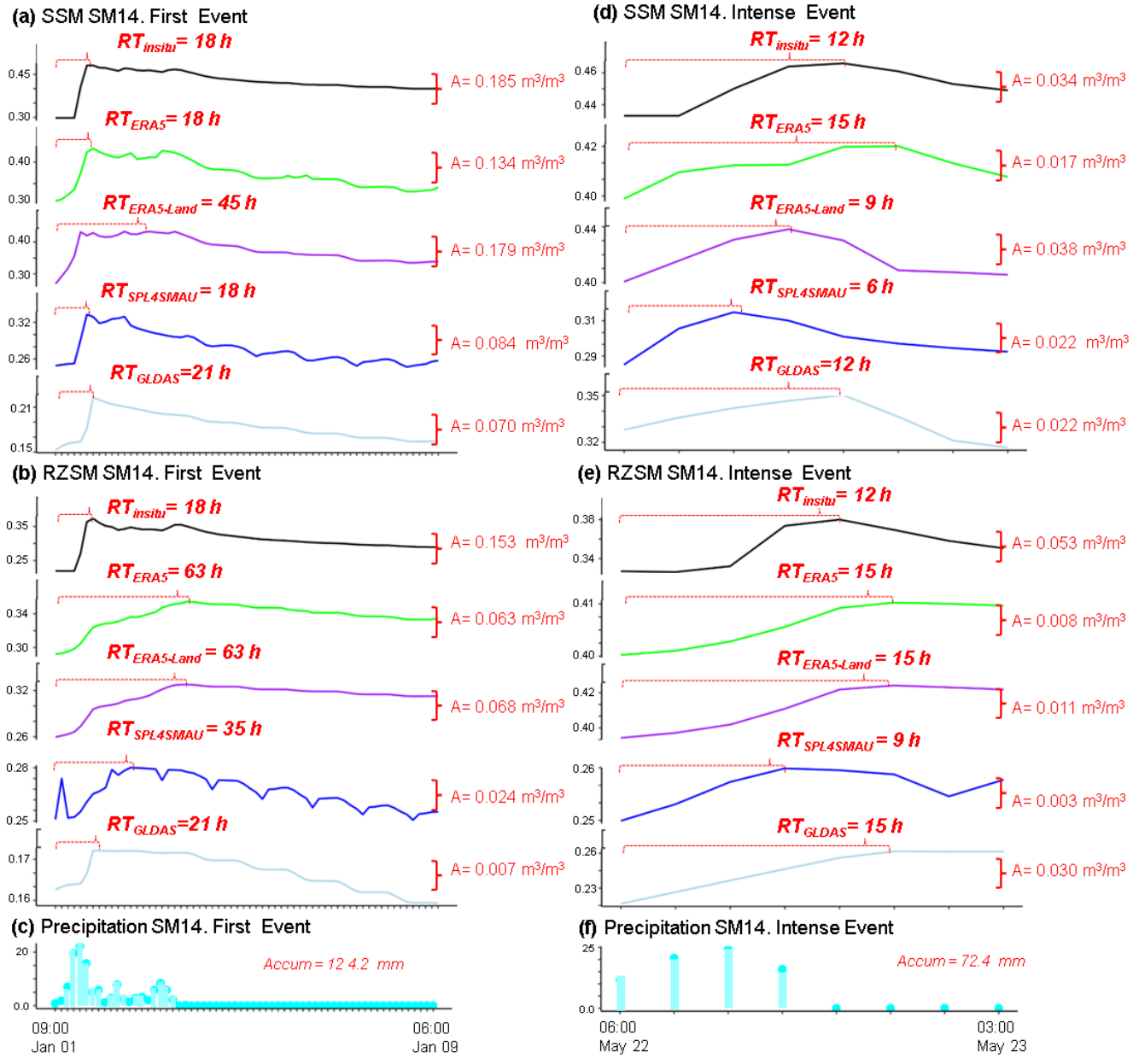

Figure 11. Amplitude (A) and rising time (RT) for the first precipitation event of 2022 in SM05 (Native Forest in Trancura). Results are shown for both surface soil moisture (SSM) and root zone soil moisture (RZSM) across observed (in situ) and gridded products. The bottom panel shows cumulative precipitation for the first event event (Accum = 124.2 mm) and Intense event (Accum = 72.4 mm).

to small-scale precipitation events. Conversely, at SM14, ERA5-Land closely followed the observed dynamics during both the

https://doi.org/10.5194/egusphere-2025-2606
Preprint. Discussion started: 28 July 2025

first and the most intense P event of the year. It accurately reproduced the amplitude (A = 0.179 vs 0.185 ^{3}/m^3 measured in situ) and response time (RT = 18 h), demonstrating its capability in more humid ecosystems.

Figure 12 confirms a recurring tendency among gridded products to simulate SM increases at northern sites that were not observed in situ. This discrepancy may be attributed to the mismatch between the coarse spatial resolution of the P fields used in land surface models and the localized P measurements recorded by individual rain gauges, which can induce artificial SM responses. For instance, ERA5-Land assimilates multiple satellite- and radar-based P sources (e.g., AMSR-2, GPM, TRMM, FY-3C) (Liu et al., 2024). However, a direct comparison between these gridded P estimates and in situ observations was beyond the scope of this work.

Figure 13 shows that, during the first P event of the year, gridded datasets generally underestimated the amplitude of in situ SM responses, particularly in northern arid ecosystems. Although estimates of rising time were somewhat closer to in situ observations, substantial variability remained among products. Our findings confirm the difficulty of accurately representing rapid infiltration and retention processes in arid environments, where P events are infrequent and exhibit a high spatial and temporal variability, as already discussed in previous studies (Lal et al., 2022; Dai et al., 2022). Moreover, while the 3-hourly temporal resolution of the datasets may be adequate for capturing large-scale SM dynamics, it might be not goo enough to resolve short-term fluctuations associated with high-intensity P events. Previous studies have shown that reanalysis products tend to smooth out high-frequency variability, potentially missing short-lived anomalies in SM response (e.g. Zheng et al., 2024).

To better understand the sources of discrepancy between gridded and in situ SM observations, future work should compare P inputs from gridded datasets with in situ observations, thus enhancing the performance and regional applicability of gridded products in poorly monitored, and ecohydrologically heterogeneous regions.

4.3.2 Regional performance

In order to provide a regional summary (i.e., arid north vs humid south) of the capability of each gridded dataset of reproducing the in situ SM signature, figures 12 and 13 show boxplots summarising the amplitude (panels a and b in each figure) and rising times (panels c and d in each figure) for SSM and RZSM during the first P event and the most intense P event of the year, respectively.

Figure 12a) shows that in situ SSM amplitudes presented lower median values and reduced variability in the arid north compared to the humid south. Most gridded datasets overestimated both the median amplitude and its variability relative to in situ data. Additionally, all gridded datasets, except SPL4SMAU, showed lower median SSM amplitudes in the south than in the north, which contrasts with in situ observations. Figure 12b illustrates that rising times for SSM were generally shorter in the north than in the south, consistent across both in situ observations and all gridded datasets. The median in situ rising times were about 1 h in the north and 25 h in the south, while gridded datasets report median rising times ranging from 15 to 25 h.

A similar pattern was observed for RZSM. Figure 12c shows that in situ RZSM amplitudes were lower and less variable in the north. Most gridded datasets overestimated the in situ amplitudes, with median values about 0.05 m^3/m^3 for all gridded datasets vs less than 0.015 m^3/m^3 for in situ measurements. In terms of variability, ERA5 and ERA5-Land underestimated

https://doi.org/10.5194/egusphere-2025-2606
Preprint. Discussion started: 28 July 2025

in situ variability in the north but aligned more closely with them in the south. In contrast, SPL4SMAU and GLDAS-Noah underestimated in situ variability in both regions. Finally, Figure 12d shows that rising times in the root zone followed a regional pattern similar to SSM, with shorter times in the north across both observation types. Median rising times from in situ data were about 10 h in the north and 30 h in the south, while gridded datasets showed median values ranging from 22 to 37 h.

Figure 13 presents results analogous to those in Figure 12, but for the amplitudes (panels a and b) and rising times (panels c and d) of SSM and RZSM in response to the most intense precipitation (P) event of the year.

Figure 13a shows that in situ SSM amplitudes presented lower median values and reduced variability in the arid north compared to the humid south. Unlike the response to the first P event, most gridded datasets underestimated both the amplitude and its variability, with the exception of ERA5 in the north, which was more closely aligned with the in situ observations. In the south, ERA5 and GLDAS-Noah underestimated both the median amplitude and their variability, whereas ERA5-Land and SPL4SMAU overestimated the median values and presented similar levels of variability in both regions. In contrast to the first event of the year, Figure 13b indicates that SSM rising times were generally shorter in the south than in the north, a pattern observed in both in situ data and all gridded datasets but GLDAS-Noah. Median rising times from in situ observations were about 15 h in the north and 10 h in the south, while gridded datasets presented values ranging from 10 to 18 h.

Figure 13c shows that in situ RZSM amplitudes were lower and more variable in the north than in the south. All gridded datasets substantially underestimated the in situ median amplitudes, with gridded values ranging from 0.007 to 0.015 m^3/m^3, compared to 0.020 to 0.045 m^3/m^3 for in situ measurements. Among the datasets, ERA5 and ERA5-Land provided the estimates closest to the in situ median amplitudes in both regions. In terms of variability, all products except GLDAS-Noah showed higher variability in the north, though all (except GLDAS-Noah) underestimated the actual variability, with a more pronounced underestimation in the north. Finally, Figure 13d reveals that rising times in the root zone followed the same regional pattern observed for SSM, with shorter times in the south across all data sources. Median rising times from in situ observations were about 18 h in the north and 15 h in the south, while gridded datasets presented values ranging from 15 to 27 h.

Our results revealed consistent regional patterns in the SM responses to precipitation events, with pronounced differences in amplitudes (A) and rising times (RT) between the arid northern and humid southern sites. Some gridded products, such as SPL4SMAU and ERA5-Land, showed better agreement with in situ observations, particularly in capturing rising times. In contrast, other products, such GLDAS-Noah, presented greater discrepancies, especially in the northern sites where both A and RT had large differences with observed values. These findings highlight region-dependent variations in the performance of gridded SM datasets, which will be further examined in the following section.

4.4 Challenges of spatial and temporal comparison

Discrepancies between the spatial and temporal scales of gridded SM datasets and point-based in situ observations pose additional challenges for product evaluation. In this study, four SM products were evaluated against the Kimün-Ko network using two complementary approaches: i) a point-to-pixel time series comparison based on conventional statistical metrics of performance, and ii) an evaluation of two event-based SM response signatures. Additionally, spatial averaging of in situ data generally led to higher performance metrics for all products (Table 5).

https://doi.org/10.5194/egusphere-2025-2606
Preprint. Discussion started: 28 July 2025

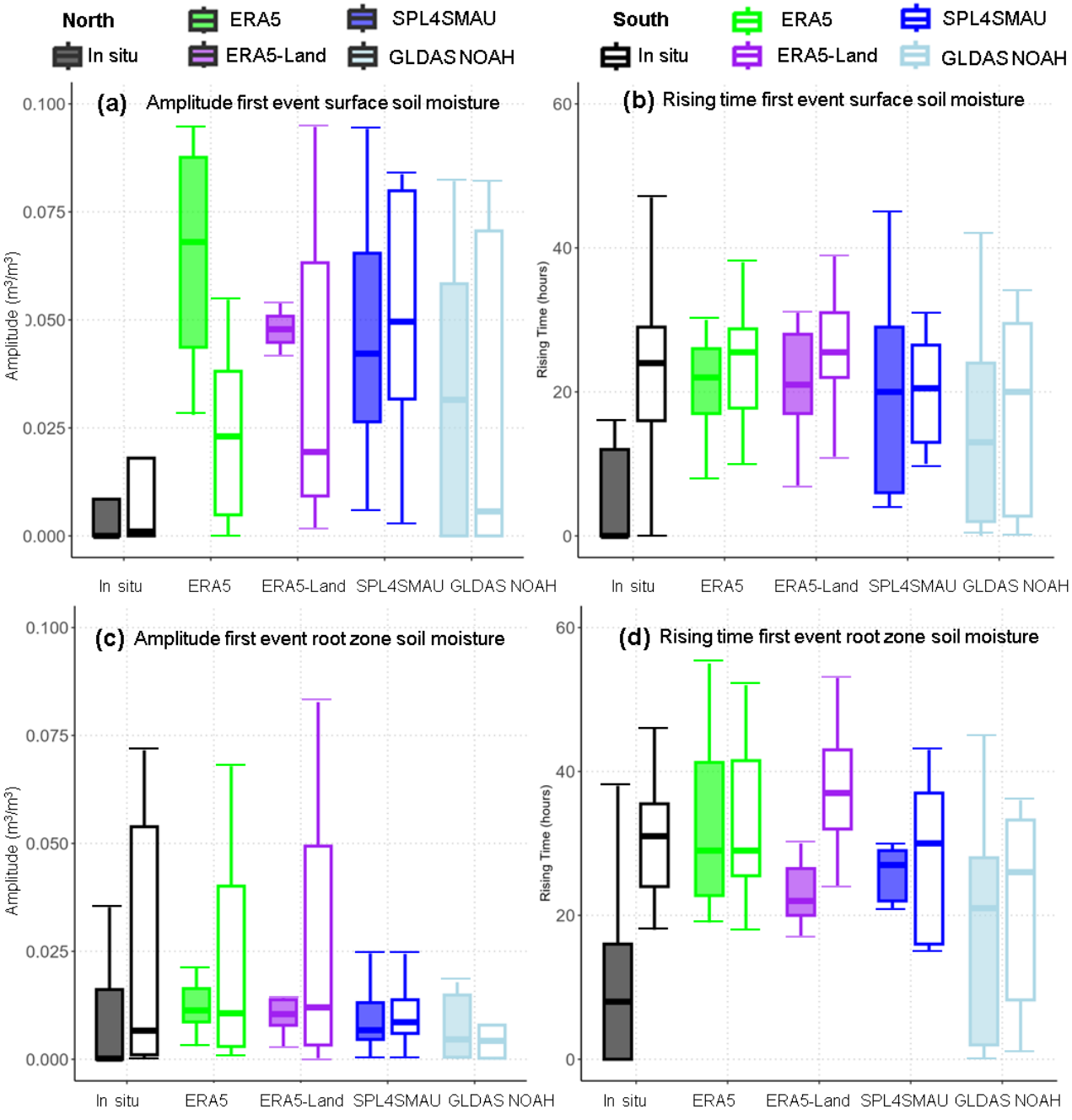

Figure 12. Boxplots summarising the amplitude (panels a and b) and rising times (panels c and d) for SSM and RZSM during the first P event of the year. Filled boxplots corresponds to the northern arid sites (SM01 to SM07) and non-filled boxplots corresponds to the southern humid sites (SM10 to SM15).

https://doi.org/10.5194/egusphere-2025-2606
Preprint. Discussion started: 28 July 2025

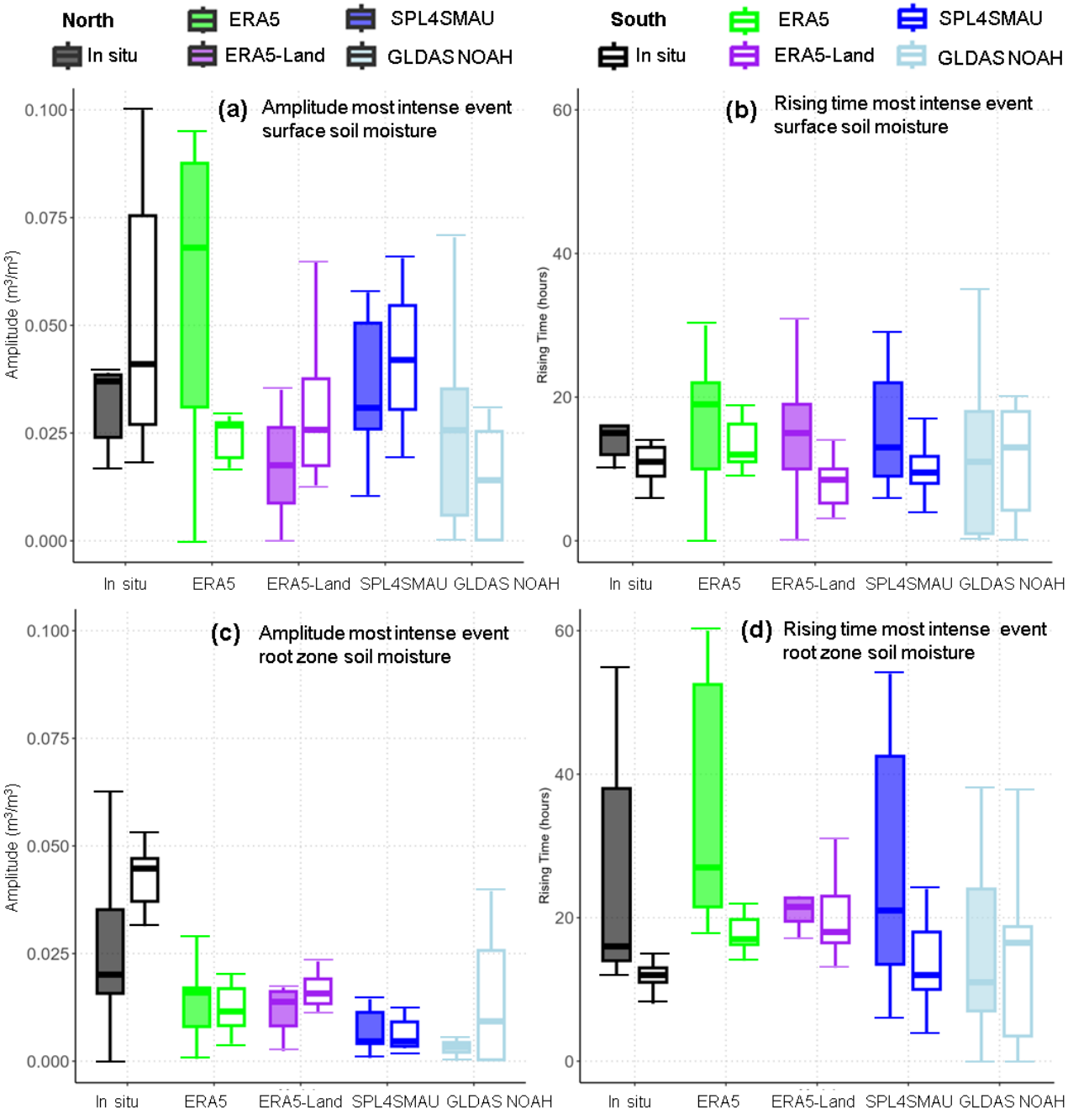

Figure 13. Boxplots summarising the amplitude (panels a and b) and rising times (panels c and d) for SSM and RZSM during the most intense P event of the year. Filled boxplots corresponds to the northern arid sites (SM01 to SM07) and non-filled boxplots corresponds to the southern humid sites (SM10 to SM15).

https://doi.org/10.5194/egusphere-2025-2606
Preprint. Discussion started: 28 July 2025

In point-to-pixel evaluations, the spatial representativeness of in situ SM measurements is limited by heterogeneity in soil properties, land cover, and P gradients. These factors can introduce representativeness errors, where point-scale observations fail to reflect the broader-scale dynamics captured by gridded datasets (Brocca et al., 2010; Xia et al., 2014; Gruber et al., 2020; Yu et al., 2024; Schmidt et al., 2024). In contrast, spatial averaging helps reduce local noise and improves alignment with regional SM patterns, thereby enhancing correlation and reducing bias (Wang and Zeng, 2012; Xia et al., 2014; Bi et al., 2016; Zheng et al., 2022a, 2024). However, recent studies indicate that higher spatial resolution does not necessarily translate into improved agreement with in situ data. For example, Schmidt et al. (2024) demonstrated that factors such as land cover, mean SM conditions, and retrieval algorithms often have a greater influence on performance than spatial resolution alone. Likewise, Degano et al. (2024) and Ortenzi et al. (2024) found that high-resolution datasets (e.g., SMAP/Sentinel-1 at 1 km and 3 km) often produced larger errors compared to coarser products (e.g., SMAP at 9 km or 36 km), particularly in the absence of local validation. These findings warn against assuming improved accuracy based solely on higher spatial resolution.

Terrain heterogeneity plays a critical role in shaping SM dynamics (Larson et al., 2022). Variations in elevation, slope, and soil composition across the study area influence water retention, infiltration, and lateral flow, thereby affecting SM estimates from both in situ sensors and gridded datasets. For instance, steeper slopes tend to enhance surface runoff and limit infiltration, while clay-rich soils typically retain more moisture than sandy soils. Incorporating these topographic and pedological factors is essential for interpreting spatial discrepancies in product performance and for improving the physical realism of SM simulations across heterogeneous ecosystems. Temporal mismatches between gridded and in situ SM further contribute to evaluation uncertainty. Most gridded SM products are produced at fixed temporal intervals (e.g., hourly, 3-hourly), which may not capture the timing of rapid SM responses to precipitation events. Such mismatch can obscure key hydrological signatures, such as response amplitude and rising time, particularly in regions characterised by high rainfall variability or pronounced seasonal transitions.

As discussed in previous sections, scale-related challenges affect the interpretation of product performance and complicate the evaluation of gridded SM datasets. While spatial aggregation can partially alleviate some representativeness issues, temporal desynchronization remains a major source of uncertainty, particularly when assessing SM dynamics at the P event scale. This limitation is especially critical when evaluating how accurately gridded products capture the timing and evolution of SM responses to P. Furthermore, in regions with sparse monitoring networks, such as many areas in the Southern Hemisphere, spatial averaging is often impractical due to the limited number of stations available per grid cell. In these contexts, one-to-one comparisons between individual in situ stations and the corresponding grid cells, as used in this study, remain a practical and essential approach for evaluating SM products in under-monitored and data-scarce ecosystems.

Finally, our study highlights the importance of incorporating deseasonalised statistical metrics in the evaluation of SM products (Schmidt et al., 2024; Peng et al., 2021), particularly in arid regions where strong seasonal fluctuations may obscure short-term dynamics. Given the lower spatial variability of SM anomalies compared to absolute values, deseasonalisation offers a more challenging basis for product assessment (Brocca et al., 2014; Albergel et al., 2012; Gruber et al., 2020; Peng et al., 2021; Schmidt et al., 2024). We recommend its routine use in future validation efforts to improve robustness and comparability across studies.

https://doi.org/10.5194/egusphere-2025-2606
Preprint. Discussion started: 28 July 2025

4.5 Influence of vegetation representation

The performance of gridded SM products is influenced not only by P inputs and soil parameterisation within land surface models, but also by how vegetation and land cover are represented. These models typically rely on global land cover datasets to define surface characteristics that affect key hydrological processes such as infiltration, evaporation, and runoff (Liu et al., 2024). However, such datasets often oversimplify vegetation structure and rooting depth—particularly in regions like Chile, where strong climatic and ecological gradients occur over short distances. These generalisations can introduce systematic biases in SM estimates, as products differ in their land cover classifications and associated vegetation parameters. For instance, GLDAS-Noah uses the AVHRR-based classification from the University of Maryland (Rui et al., 2021), while SPL4SMAU relies on MODIS-derived or GLCC-based categories (Reichle et al., 2022b). These classification schemes directly affect modelled processes such as canopy interception and transpiration, thereby influencing SM retention and temporal variability.

The previous limitations become particularly evident when comparing ecologically distinct sites (see Tables 2 and 3). In the semi-arid north (e.g., SM05), sparse vegetation and shallow-rooted species facilitate rapid infiltration and drying, resulting in brief SM responses with low amplitude and short rising times. Conversely, southern humid sites such as SM14 exhibit longer SM retention due to dense canopy cover and deep-rooted vegetation, which attenuate short-term fluctuations. These structural and functional vegetation differences are not adequately captured by current gridded SM products, leading to discrepancies in event-scale SM dynamics.

These patterns are clearly illustrated in the event-based evaluation of SM signatures. At SM05 (Figure 10), in situ observations showed no discernible SM response during the first precipitation event of the year, whereas most gridded products simulated a response, overestimating both amplitude and rising time. This indicates a limited ability to capture rapid depletion processes typical of arid shrubland ecosystems. At SM14 (Figure 11), gridded products overestimated post-event moisture retention, with rising times exceeding those observed in situ—likely due to oversimplified representations of forest transpiration and rooting depth in the land surface models.

This study contributes to better understand how gridded SM products simulate hydrological dynamics across ecologically diverse regions in the Southern Hemisphere. The evaluation of event-based SM signatures (amplitude and rising time) provided a process-oriented complement to traditional statistical metrics, allowing for a more nuanced assessment of SM dynamics. Our results reveal consistent spatial and product-specific biases and underscore the importance of regionally contextualized validation in under-monitored natural ecosystems.

5 Conclusions

This study provides a comprehensive evaluation of gridded SM products using high-temporal-resolution (3-hourly) in situ observations from the Kimün-Ko monitoring network, located across ecologically diverse native ecosystems in Chile. By assessing product performance under contrasting hydroclimatic conditions, our analysis advances the understanding of SM dynamics in data-scarce regions of the Southern Hemisphere. Our findings highlight both the potential and the limitations of

https://doi.org/10.5194/egusphere-2025-2606
Preprint. Discussion started: 28 July 2025

widely used gridded SM datasets for hydrological monitoring and modelling, and offer valuable guidance for their application in heterogeneous, under-monitored environments.

- **General performance for SSM**: Gridded SM products demonstrated moderate skill in representing SSM dynamics, with varying performance across datasets. Among the evaluated products, ERA5 and ERA5-Land consistently performed best, achieving average 3-hourly KGE′ values of 0.63 and Spearman rank correlations ranging from 0.53 in the arid north to 0.74 in the humid south. Their strong agreement with in situ temporal patterns suggests their suitability for monitoring SSM conditions in natural ecosystems. In contrast, GLDAS-Noah and SPL4SMAU showed lower performance, with a systematic tendency to overestimate SM, particularly at arid northern sites.

- **General performance for RZSM**: All gridded SM products showed stronger performance in representing RZSM than SSM, with greater consistency across monitoring sites. ERA5 and ERA5-Land achieved the highest overall performance, with mean 3-hourly KGE′ values of 0.66 and 0.70, respectively, and Spearman correlation coefficients (ρ) above 0.5 for deseasonalised time series at all monitoring sites. This strong performance likely reflects their capacity to capture the slower, more buffered dynamics of deeper soil layers, which are less sensitive to short-term variability. In contrast, GLDAS-Noah and SPL4SMAU showed notable deficiencies in reproducing RZSM patterns in natural ecosystems, with a low average KGE′ of 0.27 and poor correlation with in situ measurements.

- **Enhanced performance of ERA5 and ERA5-Land in humid ecosystems**: At the humid southern monitoring sites, ERA5 and ERA5-Land consistently outperformed other gridded products in capturing both SSM and RZSM dynamics. Their performance was particularly robust during wetter periods, with ERA5-Land achieving KGE′ values of 0.83 for SSM and 0.87 for RZSM, among the highest obtained for all the monitoring sites of the Kimün-Ko network. These results highlight the effectiveness of ERA5 and ERA5-Land in representing SM variability in humid ecosystems, where frequent P events and higher soil moisture levels prevail.

- **Challenges in representing SM dynamics in arid ecosystems**: In the northern arid ecosystems, all gridded products consistently overestimated both the amplitude and rising time of SSM and RZSM during the first precipitation event of the year. Across gridded datasets, amplitude overestimations exceeded 0.02 m^3/m^3, and rising times were overestimated by more than 20 hours (ca. 100%). Although SPL4SMAU showed comparatively better performance in arid sites based on statistical metrics such as ubRMSE and KGE′, its Spearman rank correlation exhibited substantial variability across monitoring locations, indicating inconsistencies in capturing temporal dynamics.

- **Improved performance during intense precipitation events**: Gridded SM products demonstrated better agreement with in situ observations during intense precipitation events compared to the first dry event of the year. In the northern arid ecosystems, amplitude overestimations were reduced to approximately 0.01 m^3/m^3, and rising time overestimation decreased by around 10 hours (∼50%). Similarly, in the southern humid sites, both amplitude and rising time discrepancies were smaller than those observed during the first precipitation event. These findings suggest that product performance improves under wetter conditions, likely due to more pronounced and sustained SM levels.

https://doi.org/10.5194/egusphere-2025-2606
Preprint. Discussion started: 28 July 2025

– **Deseasonalised metrics for soil moisture products evaluation**: The use of Spearman rank correlation (ρ) applied to deseasonalised time series proved effective in identifying discrepancies between observed and gridded SM estimates. This approach was particularly valuable in arid regions, where strong seasonal patterns can obscure short-term SM dynamics. In contrast, humid regions, characterised by more frequent P events, exhibited weaker seasonality, reducing the relative impact of deseasonalistion.

– **Complementary value of SM signatures in SM evaluations**: While conventional statistical metrics of performance, such as KGE', suggest acceptable to good performance across gridded SM datasets, event-based analysis of SM signatures (amplitude and rising times) revealed systematic discrepancies not captured by these aggregate statistics. For instance, ERA5-Land, which performed well in humid ecosystems, presented important timing and magnitude biases under dry conditions during the first P precipitation event of the year. These findings demonstrate that SM signatures offer valuable and complementary diagnostic insights beyond statistical metrics, and highlight the importance of incorporating ecosystem-specific evaluation approaches when assessing SM dataset performance.

6 Concluding remarks

Despite inherent spatial uncertainties and dataset limitations, this study provides valuable contributions by: i) offering a comprehensive evaluation of gridded SM datasets in natural ecosystems of the Southern Hemisphere, regions that remain largely under-monitored and under-evaluated in global studies; and ii) presenting an exhaustive assessment of both surface and root-zone SM responses to P events, revealing key spatial patterns and product-specific strengths and limitations.

Code availability. The code that support the findings of this study are available from the corresponding author, MZB, upon reasonable request.

Data availability. The soil moisture observations from Kimün-Ko SM monitoring network are available at https://chi2.ufro.cl/Datos-en/ and will soon be hosted by the ISMN (Dorigo et al., 2011); in the meantime, they can be obtained from the corresponding author (MZB). All data are freely available. ERA5 data are available at https://doi.org/10.24381/cds.adbb2d47 (Hersbach et al., 2023). ERA5-Land data can be downloaded from https://doi.org/10.24381/cds.e2161bac (Muñoz-Sabater, 2019). The SMAP L4 dataset (SPL4SMAU, Version 7) is accessible at https://doi.org/10.5067/EVKPQZ4AFC4D (Reichle et al., 2022a). GLDAS-Noah v2.1 data are provided at https://doi.org/10.5067/E7TYRXPJKWOQ (NASA/GSFC/HSL, 2020). Detailed time series and calculated statistical metrics for each site are available in the Supplementary Material S2 (Zambrano-Bigiarini et al., 2025).

https://doi.org/10.5194/egusphere-2025-2606
Preprint. Discussion started: 28 July 2025

Appendix A: Performance Metrics

Table A1. Surface soil moisture metrics: ubRMSE and PBIAS.

N	ID	ubRMSE (m^3/m^3)				PBIAS (%)			
		ERA5	ERA5Land	SPL4SMAU	GLDAS-Noah	ERA5	ERA5Land	SPL4SMAU	GLDAS-Noah
1	SM01	0.065	0.051	0.034	0.059	30.1	57.1	-33.5	21.5
2	SM02	0.070	0.061	0.043	0.058	90.7	95.7	-3.1	107.5
3	SM04	0.063	0.067	0.047	0.067	-5.1	21.0	-47.4	42.7
4	SM05	0.066	0.077	0.046	0.057	23.4	20.0	-35.1	35.4
5	SM07	0.080	0.077	0.052	0.049	54.2	75.1	4.1	42.8
6	SM15	0.039	0.046	0.040	0.034	-49.8	-3.5	14.3	-26.6
7	SM10	0.051	0.050	0.061	0.048	59.5	57.1	26.7	0.3
8	SM11	0.044	0.051	0.046	0.058	96.6	91.3	29.4	35.4
9	SM12	0.037	0.044	0.040	0.068	-8.5	-10.2	-46.8	-35.1
10	SM14	0.033	0.037	0.049	0.065	-6.6	-6.7	-25.5	-32.6

Colored according to interpretation criteria (defined in Table 4): E = Excellent (Green), G = Good (Yellow), S = Satisfactory (Orange), B = Bad (Red).

Table A2. Surface soil moisture metrics: Spearman correlation (ρ) and Kling-Gupta Efficiency (KGE).

N	ID	ρ				KGE			
		ERA5	ERA5Land	SPL4SMAU	GLDAS-Noah	ERA5	ERA5Land	SPL4SMAU	GLDAS-Noah
1	SM01	0.34	0.29	0.06	-0.37	0.46	0.27	0.56	0.36
2	SM02	0.31	0.37	0.06	-0.31	0.06	0.00	0.42	-0.31
3	SM04	0.37	0.36	-0.06	-0.29	0.26	0.43	0.27	0.15
4	SM05	0.38	0.37	0.07	-0.15	0.46	0.30	0.38	0.31
5	SM07	0.11	0.27	0.55	0.32	0.36	0.19	0.58	0.35
6	SM15	0.81	0.85	0.68	0.61	0.41	0.62	0.80	0.67
7	SM10	0.61	0.64	0.58	0.58	0.19	0.28	0.38	0.78
8	SM11	0.38	0.41	0.25	0.16	-0.11	0.03	0.35	0.54
9	SM12	0.76	0.69	0.42	0.44	0.63	0.47	0.16	-0.58
10	SM14	0.71	0.68	0.53	0.46	0.88	0.85	0.61	0.00

Colored according to interpretation criteria (defined in Table 4): E = Excellent (Green), G = Good (Yellow), S = Satisfactory (Orange), B = Bad (Red).

Author contributions. MZB and MG conceptualised the research. DNI downloaded and processed all the gridded and in situ SM data. All authors agreed on the methodology. DNI carried out the formal analysis under the guidance of MZB and MG. DNI developed the R code to analyse all the data and created all the figures, with contributions from MG and MZ. DNI wrote an early draft with contributions from MG and MZB. MZB and MG contributed to the interpretation of the results. MZB and MG were in charge of funding acquisition, project administration and supervision. MZB edited the final manuscript submitted to HESS based on several drafts elaborated by all co-authors.

https://doi.org/10.5194/egusphere-2025-2606
Preprint. Discussion started: 28 July 2025

Table A3. Root zone soil moisture metrics: ubRMSE and PBIAS.

		ubRMSE (m^3/m^3)				PBIAS (%)			
		ERA5	ERA5Land	SPL4SMAU	GLDAS-Noah	ERA5	ERA5Land	SPL4SMAU	GLDAS-Noah
1	SM01	0.024	0.015	0.023	0.043	68.10	46.00	-9.70	7.90
2	SM02	0.018	0.009	0.029	0.050	132.30	101.90	15.80	46.20
3	SM04	0.029	0.024	0.040	0.051	-11.10	-7.50	-42.30	-0.30
4	SM05	0.029	0.039	0.034	0.040	60.60	45.80	3.90	47.00
5	SM07	0.036	0.047	0.031	0.024	44.30	40.60	-10.80	8.90
6	SM15	0.026	0.047	0.041	0.030	-44.10	0.10	35.60	-35.40
7	SM10	0.036	0.032	0.053	0.045	39.40	34.40	15.50	-20.60
8	SM11	0.030	0.039	0.039	0.046	7.60	2.00	-17.10	-34.80
9	SM12	0.019	0.033	0.039	0.051	-10.30	-13.70	-46.60	-43.50
10	SM14	0.021	0.028	0.040	0.052	25.60	23.10	-6.00	-20.00

Colored according to interpretation criteria (defined in Table 4): E = Excellent (Green), G = Good (Yellow), S = Satisfactory (Orange), B = Bad (Red).

Table A4. Root zone soil moisture metrics: Spearman correlation (ρ) and Kling-Gupta Efficiency (KGE).

N	ID	ρ				KGE			
		ERA5	ERA5Land	SPL4SMAU	GLDAS	ERA5	ERA5Land	SPL4SMAU	GLDAS
1	SM01	0.79	0.92	0.08	-0.68	0.17	0.37	0.66	0.36
2	SM02	0.68	0.97	0.04	-0.62	-0.45	-0.13	0.33	0.07
3	SM04	0.74	0.93	-0.24	-0.53	0.73	0.83	0.25	0.30
4	SM05	0.81	0.76	-0.18	-0.46	0.25	0.37	0.27	0.09
5	SM07	0.26	0.40	0.61	0.37	0.36	0.51	0.70	0.77
6	SM15	0.57	0.79	0.65	0.60	0.45	0.40	0.61	0.02
7	SM10	0.77	0.82	0.59	0.62	0.36	0.55	0.50	0.51
8	SM11	0.48	0.62	0.51	0.47	0.74	0.46	0.50	-0.61
9	SM12	0.88	0.74	0.33	0.57	0.84	0.51	0.39	-0.61
10	SM14	0.81	0.73	0.52	0.62	0.62	0.73	0.66	0.24

Colored according to interpretation criteria (defined in Table 4): E = Excellent (Green), G = Good (Yellow), S = Satisfactory (Orange), B = Bad (Red).

Competing interests. We declare that no competing interests are present in the elaboration of this manuscript.

Disclaimer. Our results contain modified Copernicus Climate Change Service information 2020. Neither the European Commission nor ECMWF is responsible for any use that may be made of the Copernicus information or data it contains.

Acknowledgements. The authors acknowledge the support from the following projects: ANID Fondecyt Regular 1212071 and 1210932, ANID-PCI NSFC190018, and ANID-FONDAP 1523A0002.

https://doi.org/10.5194/egusphere-2025-2606
Preprint. Discussion started: 28 July 2025

Financial support

This research has been supported by the Chilean Agencia Nacional de Investigación y Desarrollo (ANID) through the following projects: ANID-Fondecyt Regular 1212071 and 1210932, ANID-PCI NSFC 190018, and ANID-FONDAP 1523A0002.

https://doi.org/10.5194/egusphere-2025-2606
Preprint. Discussion started: 28 July 2025

References

Adler, R. F., Gu, G., Huffman, G. J., Sapiano, M. R., and Wang, J.-J.: GPCP and the Global Characteristics of Precipitation, Satellite Precipitation Measurement: Volume 2, pp. 677–697, https://doi.org/10.1007/978-3-030-35798-6_11, 2020.

Al-Yahyai, R., Schaffer, B., Davies, F. S., and Munoz-Carpena, R.: Characterization of soil-water retention of a very gravelly loam soil varied with determination method, Soil Science, 171, 85–93, https://doi.org/10.1097/01.ss.0000187372.53896.9d, 2006.

Albergel, C., De Rosnay, P., Gruhier, C., Muñoz-Sabater, J., Hasenauer, S., Isaksen, L., Kerr, Y., and Wagner, W.: Evaluation of remotely sensed and modelled soil moisture products using global ground-based in situ observations, Remote Sensing of Environment, 118, 215–226, https://doi.org/10.1016/j.rse.2011.11.017, 2012.

Alvarez-Garreton, C., Mendoza, P. A., Boisier, J. P., Addor, N., Galleguillos, M., Zambrano-Bigiarini, M., Lara, A., Puelma, C., Cortes, G., Garreaud, R., et al.: The CAMELS-CL dataset: catchment attributes and meteorology for large sample studies–Chile dataset, Hydrology and Earth System Sciences, 22, 5817–5846, https://doi.org/10.5194/hess-22-5817-2018, 2018.

Andaryani, S., Nourani, V., Ball, J., Jahanbakhsh Asl, S., Keshtkar, H., and Trolle, D.: A comparison of frameworks for separating the impacts of human activities and climate change on river flow in existing records and different near-future scenarios, Hydrological Processes, 35, e14 301, https://doi.org/10.1002/hyp.14301, 2021.

Araki, R., Branger, F., Wiekenkamp, I., and McMillan, H.: A signature-based approach to quantify soil moisture dynamics under contrasting land-uses, Hydrological Processes, 36, https://doi.org/10.1002/hyp.14553, 2022.

Araki, R., Mu, Y., and McMillan, H.: Evaluation of GLDAS soil moisture seasonality in arid climates, Hydrological Sciences Journal, 68, 1109–1126, https://doi.org/10.1080/02626667.2023.2206032, 2023.

Arino, O., Ramos Perez, J. J., Kalogirou, V., Bontemps, S., Defourny, P., and Van Bogaert, E.: Global Land Cover Map for 2009 (GlobCover 2009), https://doi.org/10.1594/PANGAEA.787668, dataset, 2012.

Balocchi, F., Galleguillos, M., Rivera, D., Stehr, A., Arumi, J. L., Pizarro, R., Garcia-Chevesich, P., Iroumé, A., Armesto, J. J., Hervé-Fernández, P., et al.: Forest hydrology in Chile: Past, present, and future, Journal of Hydrology, 616, 128 681, https://doi.org/10.1016/j.jhydrol.2022.128681, 2023.

Beaudoing, H., Rodell, M., and NASA/GSFC/HSL: GLDAS Noah Land Surface Model L4 3 hourly 0.25×0.25 degree V2.1, https://doi.org/10.5067/E7TYRXPJKWOQ, 2020.

Beck, H. E., Pan, M., Miralles, D. G., Reichle, R. H., Dorigo, W. A., Hahn, S., Sheffield, J., Karthikeyan, L., Balsamo, G., Parinussa, R. M., et al.: Evaluation of 18 satellite-and model-based soil moisture products using in situ measurements from 826 sensors, Hydrology and Earth System Sciences, 25, 17–40, https://doi.org/10.5194/hess-25-17-2021, 2021.

Beck-Broichsitter, S., Rizvi, Z. H., Horn, R., and Wuttke, F.: Effect of gravel content on soil water retention characteristics and thermal capacity of sandy and silty soils, Journal of Hydrology and Hydromechanics, 71, 1–10, https://doi.org/10.2478/johh-2023-0001, 2023.

Bi, H., Ma, J., Zheng, W., and Zeng, J.: Comparison of soil moisture in GLDAS model simulations and in situ observations over the Tibetan Plateau, Journal of Geophysical Research: Atmospheres, 121, 2658–2678, https://doi.org/10.1002/2015jd024131, 2016.

Bown, H. E., Fuentes, J. P., and Martínez, A. M.: Assessing water use and soil water balance of planted native tree species under strong water limitations in Northern Chile, New Forests, 49, 871–892, https://doi.org/10.1007/s11056-018-9689-6, 2018.

Branger, F. and McMillan, H. K.: Deriving hydrological signatures from soil moisture data, Hydrological Processes, 34, 1410–1427, https://doi.org/10.1002/hyp.13645, 2020.

https://doi.org/10.5194/egusphere-2025-2606
Preprint. Discussion started: 28 July 2025

Brocca, L., Melone, F., Moramarco, T., and Morbidelli, R.: Spatial-temporal variability of soil moisture and its estimation across scales, Water Resources Research, 46, https://doi.org/10.1029/2009WR008016, 2010.

Brocca, L., Zucco, G., Mittelbach, H., Moramarco, T., and Seneviratne, S. I.: Absolute versus temporal anomaly and percent of saturation soil moisture spatial variability for six networks worldwide, Water Resources Research, 50, 5560–5576, https://doi.org/10.1002/2014WR015684, 2014.

Brocca, L., Gaona, J., Bavera, D., Fioravanti, G., Puca, S., Ciabatta, L., Filippucci, P., Mosaffa, H., Esposito, G., Roberto, N., et al.: Exploring the actual spatial resolution of 1 km satellite soil moisture products, Science of the Total Environment, 945, 174 087, https://doi.org/10.1016/j.scitotenv.2024.174087, 2024.

Chang, L.-L., Yuan, R., Gupta, H. V., Winter, C. L., and Niu, G.-Y.: Why is the terrestrial water storage in dryland regions declining? A perspective based on gravity recovery and climate experiment satellite observations and Noah land surface model with multiparameterization schemes model simulations, Water Resources Research, 56, e2020WR027 102, https://doi.org/10.1029/2020wr027102, 2020.

Colliander, A., Jackson, T. J., Chan, S., O'Neill, P., Bindlish, R., Cosh, M., Caldwell, T., Walker, J., Berg, A., McNairn, H., et al.: An assessment of the differences between spatial resolution and grid size for the SMAP enhanced soil moisture product over homogeneous sites, Remote sensing of environment, 207, 65–70, https://doi.org/10.1016/j.rse.2018.02.006, 2018.

Dai, L., Fu, R., Guo, X., Du, Y., Zhang, F., and Cao, G.: Soil moisture variations in response to precipitation across different vegetation types on the northeastern Qinghai-Tibet plateau, Frontiers in Plant Science, 13, 854 152, https://doi.org/10.3389/fpls.2022.854152, 2022.

Degano, M. F., Beninato, S., Holzman, M. E., Bayala, M. I., Rivas, R. E., and Massari, C.: Soil Moisture: analysis of SMAP satellite products in plain zones, in: 2024 IEEE Biennial Congress of Argentina (ARGENCON), pp. 1–8, IEEE, https://doi.org/10.1109/ARGENCON62399.2024.10735898, 2024.

Dinamarca, D. I., Galleguillos, M., Seguel, O., and Faúndez Urbina, C.: CLSoilMaps: a national soil gridded database of physical and hydraulic soil properties for Chile, Scientific Data, 10, 630, https://doi.org/s41597-023-02536-x, 2023.

Dorigo, W., Wagner, W., Hohensinn, R., Hahn, S., Paulik, C., Xaver, A., Gruber, A., Drusch, M., Mecklenburg, S., Van Oevelen, P., et al.: The International Soil Moisture Network: a data hosting facility for global in situ soil moisture measurements, Hydrology and Earth system sciences, 15, 1675–1698, https://doi.org/10.5194/hess-15-1675-2011, 2011.

Dorigo, W., Himmelbauer, I., Aberer, D., Schremmer, L., Petrakovic, I., Zappa, L., Preimesberger, W., Xaver, A., Annor, F., Ardö, J., et al.: The International Soil Moisture Network: serving Earth system science for over a decade, Hydrology and Earth System Sciences Discussions, 2021, 1–83, https://doi.org/10.5194/hess-25-5749-2021, 2021.

Dunkerley, D. L.: Rainfall intensity bursts and the erosion of soils: An analysis highlighting the need for high temporal resolution rainfall data for research under current and future climates, Earth Surface Dynamics, 7, 345–360, https://doi.org/10.5194/esurf-7-345-2019, 2019.

Dy, C. Y. and Fung, J. C. H.: Updated global soil map for the Weather Research and Forecasting model and soil moisture initialization for the Noah land surface model, Journal of Geophysical Research: Atmospheres, 121, 8777–8800, https://doi.org/10.1002/2015JD024558, 2016.

Entekhabi, D., Njoku, E. G., O'Neill, P. E., Kellogg, K. H., Crow, W. T., Edelstein, W. N., Entin, J. K., Goodman, S. D., Jackson, T. J., Johnson, J., Kimball, J., Piepmeier, J. R., Koster, R. D., Martin, N., McDonald, K. C., Moghaddam, M., Moran, S., Reichle, R., Shi, J. C., Spencer, M. W., Thurman, S. W., Tsang, L., and Van Zyl, J.: The Soil Moisture Active Passive (SMAP) Mission, Proceedings of the IEEE, 98, 704–716, https://doi.org/10.1109/JPROC.2010.2043918, 2010a.

https://doi.org/10.5194/egusphere-2025-2606
Preprint. Discussion started: 28 July 2025

Entekhabi, D., Njoku, E. G., O'neill, P. E., Kellogg, K. H., Crow, W. T., Edelstein, W. N., Entin, J. K., Goodman, S. D., Jackson, T. J., Johnson, J., et al.: The soil moisture active passive (SMAP) mission, Proceedings of the IEEE, 98, 704–716, https://doi.org/10.1109/JPROC.2010.2043918, 2010b.

Entekhabi, D., Yueh, S., O'Neill, P., Kellogg, K., Allen, A., Bindlish, R., Brown, M., Chan, S., Colliander, A., Crow, W., Das, N., De Lannoy, G., Dunbar, R., Edelstein, W., Entin, J., Escobar, V., Goodman, S., Jackson, T., Jai, B., Johnson, J., Kim, E., Kim, S., Kimball, J., Koster, R., Leon, A., McDonald, K., Moghaddam, M., Mohammed, P., Moran, S., Njoku, E., Piepmeier, J., Reichle, R., Rogez, F., Shi, J., Spencer, M., Thurman, S., Tsang, L., Van Zyl, J., Weiss, B., and West, R.: SMAP Handbook: Soil Moisture Active Passive, Mapping Soil Moisture Freeze/Thaw From Space, National Aeronautics and Space Administration, Jet Propulsion Laboratory, Pasadena, California, https://api.semanticscholar.org/CorpusID:132836213, nASA Technical Report, 2014.

Evans, J. G., Ward, H., Blake, J., Hewitt, E., Morrison, R., Fry, M., Ball, L., Doughty, L., Libre, J., Hitt, O., et al.: Soil water content in southern England derived from a cosmic-ray soil moisture observing system–COSMOS-UK, Hydrological Processes, 30, 4987–4999, https://doi.org/10.1002/hyp.10929, 2016.

Frêne, C., Dörner, J., Zuniga, F., Cuevas, J. G., Alfaro, F. D., and Armesto, J. J.: Eco-hydrological functions in forested catchments of Southern Chile, Ecosystems, 23, 307–323, https://doi.org/10.1007/s10021-019-00404-7, 2020.

Galleguillos, M., Ceballos, A., Gimeno, F., and Zambrano-Bigiarini, M.: CLDynamicLandCover, Data file available at Zenodo, https://doi.org/10.5281/zenodo.13153631, accessed: 2025-02-01, 2024.

Gelaro, R., McCarty, W., Suárez, M. J., Todling, R., Molod, A., Takacs, L., Randles, C. A., Darmenov, A., Bosilovich, M. G., Reichle, R., et al.: The modern-era retrospective analysis for research and applications, version 2 (MERRA-2), Journal of climate, 30, 5419–5454, https://doi.org/10.1175/JCLI-D-16-0758.1, 2017.

Google LLC: Google Earth Imagery, https://earth.google.com, accessed: 2025-02-01, 2024.

Gruber, A., De Lannoy, G., Albergel, C., Al-Yaari, A., Brocca, L., Calvet, J.-C., Colliander, A., Cosh, M., Crow, W., Dorigo, W., et al.: Validation practices for satellite soil moisture retrievals: What are (the) errors?, Remote sensing of environment, 244, 111 806, https://doi.org/10.1016/j.rse.2020.111806, 2020.

Hao, Y., Liu, Q., Li, C., Kharel, G., An, L., Stebler, E., Zhong, Y., and Zou, C. B.: Interactive effect of meteorological drought and vegetation types on root zone soil moisture and runoff in rangeland watersheds, Water, 11, 2357, https://doi.org/10.3390/w11112357, 2019.

Helsel, D. R. and Hirsch, R. M.: Statistical methods in water resources, vol. 49, Elsevier, 1993.

Hersbach, H., Bell, B., Berrisford, P., Hirahara, S., Horányi, A., Muñoz-Sabater, J., Nicolas, J., Peubey, C., Radu, R., Schepers, D., et al.: The ERA5 global reanalysis, Quarterly Journal of the Royal Meteorological Society, 146, 1999–2049, https://doi.org/10.1002/qj.3803, 2020.

Hersbach, H., Bell, B., Berrisford, P., Biavati, G., Horányi, A., Muñoz Sabater, J., Nicolas, J., Peubey, C., Radu, R., Rozum, I., Schepers, D., Simmons, A., Soci, C., Dee, D., and Thépaut, J.-N.: ERA5 hourly data on single levels from 1940 to present, https://doi.org/10.24381/cds.adbb2d47, 2023.

Huffman, G. J., Adler, R. F., Arkin, P., Chang, A., Ferraro, R., Gruber, A., Janowiak, J., McNab, A., Rudolf, B., and Schneider, U.: The global precipitation climatology project (GPCP) combined precipitation dataset, Bulletin of the american meteorological society, 78, 5–20, https://doi.org/10.1175/1520-0477(1997)078<0005:TGPCPG>2.0.CO;2, 1997.

Imaoka, K., Maeda, T., Kachi, M., Kasahara, M., Ito, N., and Nakagawa, K.: Status of AMSR2 instrument on GCOM-W1, in: Earth observing missions and sensors: Development, implementation, and characterization II, vol. 8528, pp. 201–206, SPIE, https://doi.org/10.1117/12.977774, 2012.

https://doi.org/10.5194/egusphere-2025-2606
Preprint. Discussion started: 28 July 2025

Jarvis, A., Reuter, H. I., Nelson, A., and Guevara, E.: Hole-filled SRTM for the globe Version 4, available from the CGIAR-CSI SRTM 90m Database, http://srtm.csi.cgiar.org, accessed: 2024-12-08, 2008.

Jiao, Y., Zhu, G., Lu, S., Ye, L., Qiu, D., Meng, G., Wang, Q., Li, R., Chen, L., Wang, Y., et al.: The cooling effect of oasis reservoir-riparian forest systems in arid regions, Water Resources Research, 60, e2024WR038 301, https://doi.org/10.1029/2024wr038301, 2024.

Kling, H., Fuchs, M., and Paulin, M.: Runoff conditions in the upper Danube basin under an ensemble of climate change scenarios, Journal of Hydrology, 424-425, 264–277, https://doi.org/10.1016/j.jhydrol.2012.01.011, 2012.

Lai, E. N., Wang-Erlandsson, L., Virkki, V., Porkka, M., and Van Der Ent, R. J.: Root zone soil moisture in over 25% of global land permanently beyond pre-industrial variability as early as 2050 without climate policy, Hydrology and Earth System Sciences, 27, 3999–4018, https://doi.org/10.5194/hess-27-3999-2023, 2023.

Lal, P., Singh, G., Das, N. N., Colliander, A., and Entekhabi, D.: Assessment of ERA5-land volumetric soil water layer product using in situ and SMAP soil moisture observations, IEEE Geoscience and Remote Sensing Letters, 19, 1–5, https://doi.org/10.1109/LGRS.2022.3223985, 2022.

Larson, J., Lidberg, W., Ågren, A. M., and Laudon, H.: Predicting soil moisture conditions across a heterogeneous boreal catchment using terrain indices, Hydrology and Earth System Sciences, 26, 4837–4851, 2022.

Lawrence, D. M., Fisher, R. A., Koven, C. D., Oleson, K. W., Swenson, S. C., Bonan, G., Collier, N., Ghimire, B., Van Kampenhout, L., Kennedy, D., et al.: The Community Land Model version 5: Description of new features, benchmarking, and impact of forcing uncertainty, Journal of Advances in Modeling Earth Systems, 11, 4245–4287, https://doi.org/10.1029/2010JD015140, 2019.

Liang, W.-L., Kosugi, K., and Mizuyama, T.: Soil water dynamics around a tree on a hillslope with or without rainwater supplied by stemflow, Water Resources Research, 47, https://doi.org/10.1029/2010WR009856, 2011.

Ling, X., Huang, Y., Guo, W., Wang, Y., Chen, C., and Peng, J.: Comprehensive evaluation of satellite-based and reanalysis soil moisture products using in situ observations over China, Hydrology and Earth System Sciences Discussions, 2021, 1–34, https://doi.org/10.5194/hess-25-4209-2021, 2021.

Liu, E., Zhu, Y., Calvet, J.-C., Lü, H., Bonan, B., Zheng, J., Gou, Q., Wang, X., Ding, Z., Xu, H., et al.: Evaluation of root zone soil moisture products over the Huai River basin, Hydrology and Earth System Sciences, 28, 2375–2400, https://doi.org/10.5194/hess-28-2375-2024, 2024.

Meng, C., Meng, C., Houser, P., Mitchell, K., Gayno, G., Rodell, M., Jambor, U., Gottschalck, J., Cosgrove, B., Radakovich, J., et al.: Implementation of the AFWA AGRMET Solar Radiation Scheme in GLDAS, in: AGU Fall Meeting Abstracts, vol. 2001, pp. H31D–0268, 2001.

Muñoz, A. A., Klock-Barría, K., Alvarez-Garreton, C., Aguilera-Betti, I., González-Reyes, Á., Lastra, J. A., Chávez, R. O., Barría, P., Christie, D., Rojas-Badilla, M., et al.: Water crisis in Petorca Basin, Chile: The combined effects of a mega-drought and water management, Water, 12, 648, https://doi.org/https://doi.org/10.3390/w12030648, 2020.

Muñoz-Sabater, J.: ERA5-Land hourly data from 1950 to present, Copernicus Climate Change Service (C3S) Climate Data Store (CDS) [data set], https://doi.org/10.24381/cds.e2161bac, 2019.

Muñoz-Sabater, J., Dutra, E., Agustí-Panareda, A., Albergel, C., Arduini, G., Balsamo, G., Boussetta, S., Choulga, M., Harrigan, S., Hersbach, H., et al.: ERA5-Land: A state-of-the-art global reanalysis dataset for land applications, Earth system science data, 13, 4349–4383, https://doi.org/10.5194/essd-13-4349-2021, 2021.

https://doi.org/10.5194/egusphere-2025-2606
Preprint. Discussion started: 28 July 2025

Nadeem, A. A., Zha, Y., Shi, L., Ran, G., Ali, S., Jahangir, Z., Afzal, M. M., and Awais, M.: Multi-scale assessment of SMAP level 3 and level 4 soil moisture products over the soil moisture network within the ShanDian River (SMN-SDR) Basin, China, Remote Sensing, 14, 982, https://doi.org/10.3390/rs14040982, 2022.

NASA/GSFC/HSL: GLDAS Noah Land Surface Model L4 3 hourly 0.25 x 0.25 degree V2.1, https://doi.org/10.5067/E7TYRXPJKWOQ, accessed: [2022-Jul-01], 2020.

Niu, G.-Y., Yang, Z.-L., Mitchell, K. E., Chen, F., Ek, M. B., Barlage, M., Kumar, A., Manning, K., Niyogi, D., Rosero, E., et al.: The community Noah land surface model with multiparameterization options (Noah-MP): 1. Model description and evaluation with local-scale measurements, Journal of Geophysical Research: Atmospheres, 116, https://doi.org/10.1029/2010JD015140, 2011.

Nogueira, M., Albergel, C., Boussetta, S., Johannsen, F., Trigo, I. F., Ermida, S. L., Martins, J. P. A., and Dutra, E.: Role of vegetation in representing land surface temperature in the CHTESSEL (CY45R1) and SURFEX-ISBA (v8.1) land surface models: a case study over Iberia, Geoscientific Model Development, 13, 3975–3993, https://doi.org/10.5194/gmd-13-3975-2020, 2020.

Ortenzi, S., Cencetti, C., Mincu, F.-I., Neculau, G., Chendeş, V., Ciabatta, L., Massari, C., and Di Matteo, L.: Comparing Satellite Soil Moisture Products Using In Situ Observations over an Instrumented Experimental Basin in Romania, Remote Sensing, 16, 3283, https://doi.org/10.3390/rs16173283, 2024.

Paloscia, S., Pettinato, S., Santi, E., Notarnicola, C., Pasolli, L., and Reppucci, A.: Soil moisture mapping using Sentinel-1 images: Algorithm and preliminary validation, Remote Sensing of Environment, 134, 234–248, https://doi.org/10.1016/j.rse.2013.02.027, 2013.

Parinussa, R. M., Holmes, T. R., Wanders, N., Dorigo, W. A., and de Jeu, R. A.: A preliminary study toward consistent soil moisture from AMSR2, Journal of Hydrometeorology, 16, 932–947, https://doi.org/10.1175/JHM-D-13-0200.1, 2015.

Peng, J., Tanguy, M., Robinson, E. L., Pinnington, E., Evans, J., Ellis, R., Cooper, E., Hannaford, J., Blyth, E., and Dadson, S.: Estimation and evaluation of high-resolution soil moisture from merged model and Earth observation data in the Great Britain, Remote Sensing of Environment, 264, 112 610, https://doi.org/10.1016/j.rse.2021.112610, 2021.

Räsänen, M., Merbold, L., Vakkari, V., Aurela, M., Laakso, L., Beukes, J. P., Van Zyl, P. G., Josipovic, M., Feig, G., Pellikka, P., et al.: Root-zone soil moisture variability across African savannas: From pulsed rainfall to land-cover switches, Ecohydrology, 13, e2213, https://doi.org/10.1002/eco.2213, 2020.

Reichle, R., Koster, R., De Lannoy, G., Crow, W., and Kimball, J.: Level 4 Surface and Root Zone Soil Moisture (L4_SM) Data Product, Tech. rep., NASA Goddard Space Flight Center, available at https://nsidc.org/sites/default/files/272_l4_sm_reva_web_0.pdf. Last visited: 08-May-2025, 2014.

Reichle, R. H., De Lannoy, G. J., Liu, Q., Ardizzone, J. V., Colliander, A., Conaty, A., Crow, W., Jackson, T. J., Jones, L. A., Kimball, J. S., et al.: Assessment of the SMAP level-4 surface and root-zone soil moisture product using in situ measurements, Journal of hydrometeorology, 18, 2621–2645, https://doi.org/10.1175/JHM-D-17-0063.1, 2017a.

Reichle, R. H., De Lannoy, G. J. M., Liu, Q., Koster, R. D., Kimball, J. S., Crow, W. T., Ardizzone, J. V., Chakraborty, P., Collins, D. W., Conaty, A. L., Girotto, M., Jones, L. A., Kolassa, J., Lievens, H., Lucchesi, R. A., and Smith, E. B.: Global Assessment of the SMAP Level-4 Surface and Root-Zone Soil Moisture Product Using Assimilation Diagnostics, Journal of Hydrometeorology, 18, 3217–3237, https://doi.org/10.1175/JHM-D-17-0130.1, 2017b.

Reichle, R. H., De Lannoy, G. J. M., Koster, R. D., Crow, W. T., Kimball, J. S., Liu, Q., and Bechtold, M.: SMAP L4 Global 3-hourly 9 km EASE-Grid Surface and Root Zone Soil Moisture Analysis Update, Version 7, https://doi.org/10.5067/LWJ6TF5SZRG3, [Last access: 11 Feb 2024], 2022a.

https://doi.org/10.5194/egusphere-2025-2606
Preprint. Discussion started: 28 July 2025

Reichle, R. H., Liu, Q., Koster, R. D., Ardizzone, J. V., Colliander, A., Crow, W. T., De Lannoy, G. J. M., and Kimball, J. S.: Soil Moisture Active Passive (SMAP) Project Assessment Report for Version 7 of the L4_SM Data Product, Tech. rep., Technical Report Series on Global Modeling and Data Assimilation, Vol. 58, https://nsidc.org/sites/default/files/documents/user-guide/multi_spl4smau-v007-userguide.pdf, [Last access: 11 Feb 2024], 2022b.

Rienecker, M. M., Suarez, M. J., Todling, R., Bacmeister, J., Takacs, L., Liu, H.-C., Gu, W., Sienkiewicz, M., Koster, R. D., Gelaro, R., Stajner, I., and Nielsen, J. E.: The GEOS-5 Data Assimilation System – Documentation of Versions 5.0.1, 5.1.0, and 5.2.0, Tech. rep., NASA Tech. Rep. Series on Global Modeling and Data Assimilation, https://ntrs.nasa.gov/api/citations/20120011955/downloads/20120011955.pdf, last access: 11 Feb 2024, 2008.

Rodell, M., Houser, P. R., Jambor, U., Gottschalck, J., Mitchell, K., Meng, C.-J., Arsenault, K., Cosgrove, B., Radakovich, J., Bosilovich, M., Entin*, J. K., Walker, J. P., Lohmann, D., and Toll, D.: The Global Land Data Assimilation System, Bulletin of the American Meteorological Society, vol. 85, Issue 3, pp.381-394, 85, 381–394, https://doi.org/10.1175/BAMS-85-3-381, 2004.

Rui, H., Beaudoing, H., and Loeser, C.: README Document for NASA GLDAS Version 2 Data Products, https://hydro1.gesdisc.eosdis.nasa.gov/data/GLDAS/GLDAS_NOAH025_3H.2.1/doc/README_GLDAS2.pdf, last access: 17 May 2024, 2021.

Sanchez-Mejia, Z. M. and Papuga, S. A.: Empirical modeling of planetary boundary layer dynamics under multiple precipitation scenarios using a two-layer soil moisture approach: An example from a semiarid shrubland, Water Resources Research, 53, 8807–8824, https://doi.org/10.1002/2016wr020275, 2017.

Schmidt, T., Schrön, M., Li, Z., Francke, T., Zacharias, S., Hildebrandt, A., and Peng, J.: Comprehensive quality assessment of satellite- and model-based soil moisture products against the COSMOS network in Germany, Remote Sensing of Environment, 301, 113 930, https://doi.org/10.1016/j.rse.2023.113930, 2024.

Schönauer, M., Ågren, A. M., Katzensteiner, K., Hartsch, F., Arp, P., Drollinger, S., and Jaeger, D.: Soil moisture modeling with ERA5-Land retrievals, topographic indices, and in situ measurements and its use for predicting ruts, Hydrology and Earth System Sciences, 28, 2617–2633, https://doi.org/10.5194/hess-28-2617-2024, 2024.

Seguel, O., Galleguillos, M., Dinamarca, D., Pfeiffer, M., Pérez-Quezada, J., Zambrano-Bigiarini, M., Zamorano, C., Fustos, I., and Casanova, G.: ChSPD Chilean soil profile database V2 (Version 2), https://doi.org/10.5281/zenodo.13870760, data set, 2024.

Sehgal, V., Sridhar, V., and Tyagi, A.: Stratified drought analysis using a stochastic ensemble of simulated and in-situ soil moisture observations, Journal of Hydrology, 545, 226–250, https://doi.org/10.1016/j.jhydrol.2016.12.033, 2017.

Senanayake, I. P., Yeo, I.-Y., Hancock, G. R., and Willgoose, G. R.: A decadal record of soil moisture space–time variability over a south-east Australian catchment, Hydrological Processes, 36, e14 770, https://doi.org/10.1002/hyp.14770, 2022.

Smith, A. B., Walker, J. P., Western, A. W., Young, R., Ellett, K., Pipunic, R., Grayson, R., Siriwardena, L., Chiew, F. H., and Richter, H.: The Murrumbidgee soil moisture monitoring network data set, Water Resources Research, 48, https://doi.org/10.1029/2012WR011976, 2012.

Spennemann, P. C., Rivera, J. A., Saulo, A. C., and Penalba, O. C.: A comparison of GLDAS soil moisture anomalies against standardized precipitation index and multisatellite estimations over South America, Journal of Hydrometeorology, 16, 158–171, https://doi.org/10.1175/JHM-D-13-0190.1, 2015.

Tian, J., Zhang, B., He, C., Han, Z., Bogena, H. R., and Huisman, J. A.: Dynamic response patterns of profile soil moisture wetting events under different land covers in the Mountainous area of the Heihe River Watershed, Northwest China, Agricultural and forest meteorology, 271, 225–239, https://doi.org/10.1016/j.agrformet.2019.03.006, 2019.

https://doi.org/10.5194/egusphere-2025-2606
Preprint. Discussion started: 28 July 2025

Van Den Broeke, M. S., Kalin, A., Alavez, J. A. T., Oglesby, R., and Hu, Q.: A warm-season comparison of WRF coupled to the CLM4. 0, Noah-MP, and Bucket hydrology land surface schemes over the central USA, Theoretical and Applied Climatology, 134, 801–816, https://doi.org/10.1007/s00704-017-2301-8, 2018.

Vereecken, H., Amelung, W., Bauke, S. L., Bogena, H., Brüggemann, N., Montzka, C., Vanderborght, J., Bechtold, M., Blöschl, G., Carminati, A., et al.: Soil hydrology in the Earth system, Nature Reviews Earth & Environment, 3, 573–587, https://doi.org/10.1038/s43017-022-00324-6, 2022.

Wagner, W., Hahn, S., Kidd, R., Melzer, T., Bartalis, Z., Hasenauer, S., Figa-Saldaña, J., De Rosnay, P., Jann, A., Schneider, S., et al.: The ASCAT soil moisture product: A review of its specifications, validation results, and emerging applications, Meteorologische Zeitschrift, https://doi.org/10.1127/0941-2948/2013/0399, 2013.

Wang, A. and Zeng, X.: Evaluation of multireanalysis products with in situ observations over the Tibetan Plateau, Journal of geophysical research: Atmospheres, 117, https://doi.org/10.1029/2011JD016553, 2012.

Wang, Y., Mao, J., Jin, M., Hoffman, F. M., Shi, X., Wullschleger, S. D., and Dai, Y.: Development of observation-based global multilayer soil moisture products for 1970 to 2016, Earth System Science Data, 13, 4385–4405, https://doi.org/10.5194/essd-13-4385-2021, 2021.

Wieder, W., Boehnert, J., Bonan, G., and Langseth, M.: Regridded harmonized world soil database v1. 2, Ornl Daac, https://doi.org/10.3334/ORNLDAAC/1247, 2014.

Wu, Z., Feng, H., He, H., Zhou, J., and Zhang, Y.: Evaluation of soil moisture climatology and anomaly components derived from ERA5-land and GLDAS-2.1 in China, Water Resources Management, 35, 629–643, https://doi.org/10.1007/s11269-020-02743-w, 2021.

Xi, X., Zhuang, Q., Kim, S., and Gentine, P.: Evaluating the effects of precipitation and evapotranspiration on soil moisture variability within CMIP5 using SMAP and ERA5 data, Water Resources Research, 59, e2022WR034 225, https://doi.org/10.1029/2022WR034225, 2023.

Xia, Y., Sheffield, J., Ek, M. B., Dong, J., Chaney, N., Wei, H., Meng, J., and Wood, E. F.: Evaluation of multi-model simulated soil moisture in NLDAS-2, Journal of Hydrology, 512, 107–125, https://doi.org/10.1016/j.jhydrol.2014.02.027, 2014.

Xing, Z., Fan, L., Zhao, L., De Lannoy, G., Frappart, F., Peng, J., Li, X., Zeng, J., Al-Yaari, A., Yang, K., et al.: A first assessment of satellite and reanalysis estimates of surface and root-zone soil moisture over the permafrost region of Qinghai-Tibet Plateau, Remote Sensing of Environment, 265, 112 666, https://doi.org/10.1016/j.rse.2021.112666, 2021.

Xu, X.: Evaluation of SMAP level 2, 3, and 4 soil moisture datasets over the Great Lakes region, Remote Sensing, 12, 3785, https://doi.org/10.3390/rs12223785, 2020.

Yapo, P. O., Gupta, H. V., and Sorooshian, S.: Automatic calibration of conceptual rainfall-runoff models: sensitivity to calibration data, Journal of Hydrology, 181, 23–48, https://doi.org/10.1016/00221694(95)02918-4, 1996.

Yu, Y., Malone, B. P., and Renzullo, L. J.: Empirical Upscaling of Point-scale Soil Moisture Measurements for Spatial Evaluation of Model Simulations and Satellite Retrievals, arXiv preprint arXiv:2404.05229, https://doi.org/10.1109/IGARSS53475.2024.10642763, 2024.

Zacharias, S., Bogena, H., Samaniego, L., Mauder, M., Fuß, R., Pütz, T., Frenzel, M., Schwank, M., Baessler, C., Butterbach-Bahl, K., et al.: A network of terrestrial environmental observatories in Germany, Vadose zone journal, 10, 955–973, https://doi.org/10.2136/vzj2010.0139, 2011.

Zambrano-Bigiarini, M.: hydroGOF: Goodness-of-fit functions for comparison of simulated and observed hydrological time series, https://doi.org/10.5281/zenodo.839854, r package version 0.6-0.1 . doi:10.5281/zenodo.839854, 2024.

Zambrano-Bigiarini, M., Galleguillos, M., and Daniel, N. n.-I.: Supplementary material for manuscript egusphere-2025-2606 "From grid to ground: How well do gridded products represent soil moisture dynamics in natural ecosystems during precipitation events?" by Núñez-Ibarra, Zambrano-Bigiarini and Galleguillos, https://doi.org/10.5281/zenodo.15585192, 2025.

https://doi.org/10.5194/egusphere-2025-2606
Preprint. Discussion started: 28 July 2025

Zheng, C., Jia, L., and Zhao, T.: A 21-year dataset (2000–2020) of gap-free global daily surface soil moisture at 1-km grid resolution, Scientific Data, 10, 139, https://doi.org/s41597-023-01991-w, 2023.

Zheng, J., Zhao, T., Lü, H., Shi, J., Cosh, M. H., Ji, D., Jiang, L., Cui, Q., Lu, H., Yang, K., et al.: Assessment of 24 soil moisture datasets using a new in situ network in the Shandian River Basin of China, Remote Sensing of Environment, 271, 112 891, https://doi.org/10.1016/j.rse.2022.112891, 2022a.

Zheng, Y., Bourassa, M. A., and Ali, M.: The impact of rainfall on soil moisture variability in four homogeneous rainfall zones of India during strong, weak, and normal Indian summer monsoons, Water, 14, 2788, https://doi.org/10.3390/w14182788, 2022b.

Zheng, Y., Coxon, G., Woods, R., Power, D., Rico-Ramirez, M. A., McJannet, D., Rosolem, R., Li, J., and Feng, P.: Evaluation of reanalysis soil moisture products using cosmic ray neutron sensor observations across the globe, Hydrology and Earth System Sciences, 28, 1999–2022, https://doi.org/10.5194/hess-28-1999-2024, 2024.

Zhuo, L., Dai, Q., Han, D., Chen, N., and Zhao, B.: Assessment of simulated soil moisture from WRF Noah, Noah-MP, and CLM land surface schemes for landslide hazard application, Hydrology and Earth System Sciences, 23, 4199–4218, https://doi.org/10.5194/hess-23-4199-2019, 2019.

Zomer, R. J., Xu, J., and Trabucco, A.: Version 3 of the Global Aridity Index and Potential Evapotranspiration Database, Scientific Data, 9, 409, https://doi.org/10.1038/s41597-022-01408-4, 2022.